25. **Fasshauer M, Klein J, Neumann S, Eszlinger M, Paschke R.** Adiponectin gene expression is inhibited by beta-adrenergic stimulation via protein kinase A in 3T3-L1 adipocytes. *FEBS Lett.* 2001;507:142–6.
26. **Delporte ML, Funahashi T, Takahashi M, Matsuzawa Y, Brichard SM.** Pre- and post-translational negative effect of beta-adrenoceptor agonists on adiponectin secretion: in vitro and in vivo studies. *Biochem J.* 2002;367:677–85.
27. **Yoda M, Nakano Y, Tobe T, Shioda S, Choi-Miura NH, Tomita M.** Characterization of mouse GBP28 and its induction by exposure to cold. *Int J Obes Relat Metab Disord.* 2001;25:75–83.
28. **Trayhurn P, James WP, Gurr MI.** Studies on the body composition, fat distribution and fat cell size and number of "Ad," a new obese mutant mouse. *Br J Nutr.* 1979;41:211–21.
29. **Bouillaud F, Ricquier D, Mory G, Thibault J.** Increased level of mRNA for the uncoupling protein in brown adipose tissue of rats during thermogenesis induced by cold exposure or norepinephrine infusion. *J Biol Chem.* 1984;259:11583–6.
30. **Nagase I, Yoshida T, Kumamoto K, et al.** Expression of uncoupling protein in skeletal muscle and white fat of obese mice treated with thermogenic beta 3-adrenergic agonist. *J Clin Invest.* 1996;97:2898–904.
31. **Moore KE, Dominic JA.** Tyrosine hydroxylase inhibitors. *Fed Proc.* 1971;30:859–70.
32. **Evans BA, Agar L, Summers RJ.** The role of the sympathetic nervous system in the regulation of leptin synthesis in C57BL/6 mice. *FEBS Lett.* 1999;444:149–54.
33. **Fruebis J, Tsao TS, Javorschi S, et al.** Proteolytic cleavage product of 30-kDa adipocyte complement-related protein increases fatty acid oxidation in muscle and causes weight loss in mice. *Proc Natl Acad Sci USA.* 2001;98:2005–10.
34. **Berg AH, Combs TP, Du X, Brownlee M, Scherer PE.** The adipocyte-secreted protein Acrp30 enhances hepatic insulin action. *Nat Med.* 2001;7:947–53.
35. **Yamauchi T, Kamon J, Waki H, et al.** The fat-derivedhormone adiponectin reverses insulin resistance associated with both lipoatrophy and obesity. *Nat Med.* 2001;7:941–6.
36. **Maeda N, Shimomura I, Kishida K, et al.** Diet-induced insulin resistance in mice lacking adiponectin/ACRP30. *Nat Med.* 2002;8:731–7.
37. **Qi Y, Takahashi N, Hileman SM, et al.** Adiponectin acts in the brain to decrease body weight. *Nat Med.* 2004;10:524–9.
38. **Yang X, Jansson PA, Nagaev I, et al.** Evidence of impaired adipogenesis in insulin resistance. *Biochem Biophys Res Commun.* 2004;317:1045–51.
39. **Iwaki M, Matsuda M, Maeda N, et al.** Induction of adiponectin, a fat-derived antidiabetic and antiatherogenic factor, by nuclear receptors. *Diabetes.* 2003;52:1655–63.
40. **Scherrer U, Randin D, Tappy L, Vollenweider P, Jequier E, Nicod P.** Body fat and sympathetic nerve activity in healthy subjects. *Circulation.* 1994;89:2634–40.
41. **Alvarez GE, Beske SD, Ballard TP, Davy KP.** Sympathetic neural activation in visceral obesity. *Circulation.* 2002;106: 2533–6.
42. **Egawa M, Yoshimatsu H, Bray GA.** Effects of 2-deoxy-D-glucose on sympathetic nerve activity to interscapular brown adipose tissue. *Am J Physiol.* 1989;257:R1377–85.
43. **Rahmouni K, Morgan DA, Morgan GM, et al.** Hypothalamic PI3K and MAPK differentially mediate regional sympathetic activation to insulin. *J Clin Invest.* 2004;114: 652–8.
44. **Pouliot MC, Despres JP, Nadeau A, et al.** Visceral obesity in men: associations with glucose tolerance, plasma insulin, and lipoprotein levels. *Diabetes.* 1992;41:826–34.
45. **Abate N, Garg A, Peshock RM, Stray-Gundersen J, Grundy SM.** Relationships of generalized and regional adiposity to insulin sensitivity in men. *J Clin Invest.* 1995;96: 88–98.

Neuronal Pathway from the Liver Modulates Energy Expenditure and Systemic Insulin Sensitivity

Kenji Uno,[1,2*] Hideki Katagiri,[2*†] Tetsuya Yamada,[1*] Yasushi Ishigaki,[1] Takehide Ogihara,[2] Junta Imai,[1,2] Yutaka Hasegawa,[1,2] Junhong Gao,[1,2] Keizo Kaneko,[1,2] Hiroko Iwasaki,[2] Hisamitsu Ishihara,[1] Hironobu Sasano,[3] Kouichi Inukai,[4] Hiroyuki Mizuguchi,[5] Tomoichiro Asano,[6] Masakazu Shiota,[7] Masamitsu Nakazato,[8] Yoshitomo Oka[1]

Coordinated control of energy metabolism and glucose homeostasis requires communication between organs and tissues. We identified a neuronal pathway that participates in the cross talk between the liver and adipose tissue. By studying a mouse model, we showed that adenovirus-mediated expression of peroxisome proliferator–activated receptor (PPAR)–γ2 in the liver induces acute hepatic steatosis while markedly decreasing peripheral adiposity. These changes were accompanied by increased energy expenditure and improved systemic insulin sensitivity. Hepatic vagotomy and selective afferent blockage of the hepatic vagus revealed that the effects on peripheral tissues involve the afferent vagal nerve. Furthermore, an antidiabetic thiazolidinedione, a PPARγ agonist, enhanced this pathway. This neuronal pathway from the liver may function to protect against metabolic perturbation induced by excessive energy storage.

The incidence of obesity, insulin resistance, hyperlipidemia, and hypertension, collectively referred to as the metabolic syndrome, is increasing at an alarming rate in Western cultures (*1*). Secreted humoral factors, including leptin (*2*), convey information about energy storage from adipose tissue to the central nervous system (CNS). As in adipose tissues, fat storage in the liver is dynamically changed by overall energy balance, but our understanding of how the liver transmits metabolic signals to other tissues remains incomplete. Studies of mouse models created by tissue-specific genetic engineering (*3*, *4*) or adenoviral gene transfer (*5*, *6*) have shown the importance of cross talk between tissues in the regulation of energy metabolism. Mice with tissue-specific knockout of peroxisome proliferator–activated receptor γ (PPARγ) provide an example of such intertissue communication (*7*). PPARγ activates genes involved in lipid storage and metabolism (*8*). Although PPARγ expression in the liver is low compared with that in adipose tissues (*9*), hepatic expression of PPARγ (*10*, *11*), especially that of PPARγ2 (*12*), is functionally enhanced in a number of obesity models. In addition, liver-specific disruption of PPARγ in obese (ob/ob) mice prevents hepatic steatosis but increases peripheral adiposity and decreases insulin sensitivity in muscle and fat (*13*). Thus, hepatic PPARγ2 plays important roles not only in the development of liver steatosis but also in the regulation of peripheral lipid storage and insulin sensitivity.

To investigate the mechanism by which hepatic PPARγ2 expression affects metabolism in peripheral tissues, we overexpressed PPARγ2 in the livers of C57BL/6 mice using adenoviral gene transfer. After being fed a high-fat diet for 4 weeks, the mice developed obesity-associated diabetes (*14*). The PPARγ2 adenovirus vector was then administered intravenously to mice (PPARγ2 mice). Control mice given the LacZ adenovirus (LacZ mice) showed no alterations in blood glucose levels, food intake, or plasma lipid parameters after virus administration (*14*). Systemic infusion of the PPARγ2 adenovirus into mice resulted in expression of the transgene primarily in the liver (Fig. 1A), without increased expression in peripheral tissues, including white adipose tissue (WAT) (Fig. 1B).

The livers of PPARγ2 mice were pale and enlarged as compared with those of control mice (fig. S1A). Liver weights were significantly increased (Fig. 1C) because of increased triglyceride content (Fig. 1D). Histological analysis of PPARγ2 mice revealed an abundance of large lipid droplets in the livers, without apparent inflammation or structural change (fig. S1B). Thus, hepatic PPARγ2 expression induced severe hepatic steatosis. Hepatic PPARγ2 expression enhanced the expression of lipogenesis-related genes (fig. S2), suggesting that increased uptake and synthesis of fatty acids induce severe steatosis.

In contrast, WAT in PPARγ2 mice was notably diminished in size (fig. S1A); for example, epididymal fat weight was decreased by 46.6% in PPARγ2 mice versus controls (Fig. 1E). Cell diameters in WAT and brown adipose tissue (BAT) were also markedly decreased in PPARγ2 mice (fig. S1C). The increases in body weights induced by a high-fat diet were suppressed in PPARγ2 mice (Fig. 1F). Resting oxygen consumption was increased by 29.4% in PPARγ2 mice (Fig. 1G), whereas food intake did not differ from that of LacZ mice (Fig. 1H).

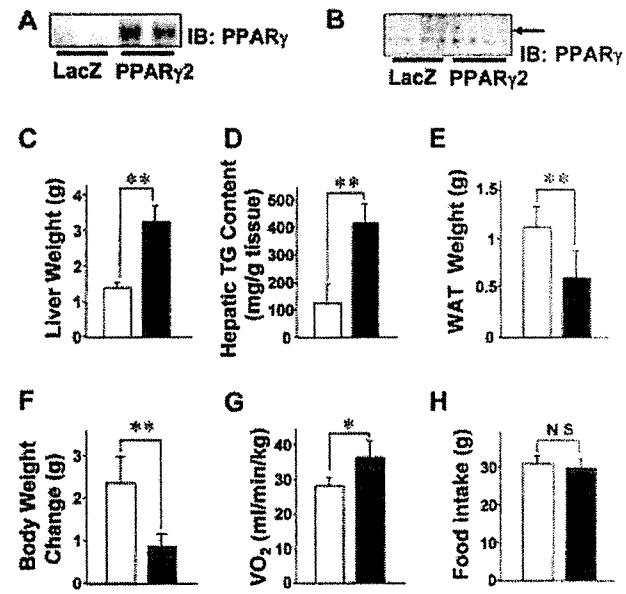

Fig. 1. Hepatic PPARγ2 expression aggravates hepatic steatosis but diminishes peripheral adiposity. (**A** and **B**) Immunoblotting (IB) with an antibody to PPARγ of liver (A) and epididymal fat (B) extracts. Liver weight (**C**), triglyceride (TG) content (**D**), and epididymal fat tissue (WAT) weights (**E**) are shown. Experiments in (A) to (E) were performed on day 7 after adenoviral administration. (**F**) Body weight changes during the 7 days after adenoviral administration. (**G**) Resting oxygen consumption (VO_2) was measured on day 3 after adenoviral injection. (**H**) Total food intake was measured for 7 days after adenoviral administration. In (C) to (H), white and black bars indicate results from LacZ mice and PPARγ2 mice, respectively. Significance as compared to LacZ mice is indicated (**$P < 0.01$ and *$P < 0.05$) by an unpaired t test. NS, not significant.

[1]Division of Molecular Metabolism and Diabetes, [2]Advanced Therapeutics for Metabolic Diseases, Center for Translational and Advanced Animal Research, [3]Department of Pathology, Tohoku University Graduate School of Medicine, Sendai 980–8575, Japan. [4]The Fourth Department of Internal Medicine, Saitama Medical School, Moroyama, Iruma-gun, Saitama 350–0495, Japan. [5]Laboratory of Gene Transfer and Regulation, National Institute of Biomedical Innovation, Osaka 567–0085, Japan. [6]Department of Physiological Chemistry and Metabolism, University of Tokyo, Tokyo 113–8655, Japan. [7]Department of Molecular Physiology and Biophysics, Vanderbilt University Medical Center, Nashville, TN 37232, USA. [8]Third Department of Internal Medicine, Miyazaki Medical College, University of Miyazaki, Kiyotake, Miyazaki 889–1692, Japan.

*These authors contributed equally to this work.
†To whom correspondence should be addressed E-mail: katagiri@mail.tains.tohoku.ac.jp

Thus, hepatic PPARγ2 expression increased systemic energy expenditure, thereby suppressing high-fat diet–induced weight gain.

Control mice were hyperglycemic, hyperinsulinemic, and hyperleptinemic in response to a 5-week-long high-fat diet. Hepatic PPARγ2 expression decreased fasting blood glucose and insulin levels (Fig. 2A), indicating markedly improved systemic insulin sensitivity. As shown in Fig. 2B, PPARγ2 mice also showed a 79% reduction in serum leptin levels. Although serum adiponectin levels were similar to those in control mice, tumor necrosis factor–α (TNF-α) levels were significantly decreased in PPARγ2 mice. These findings are consistent with a reduction in peripheral adiposity.

Glucose tolerance (Fig. 2C) and insulin tolerance (Fig. 2D) tests showed that hepatic expression of PPARγ2 markedly improved insulin sensitivity and glucose tolerance. Furthermore, improved insulin sensitivity in muscle (fig. S3A) and epididymal fat tissue (fig. S3B) was confirmed by enhanced tyrosine phosphorylation of the insulin receptor and insulin receptor substrate–1 in response to insulin administration. Thus, hepatic PPARγ2 expression clearly exerts remote beneficial effects on insulin sensitivity in muscle and WAT. Although insulin sensitivity in the liver was impaired (fig. S3C), hepatic PPARγ coactivator (PGC)–1α and hepatic phosphoenolpyruvate carboxykinase (PEPCK) expression was decreased (Fig. 2E), suggesting decreased hepatic glucose output.

To further examine insulin sensitivity and endogenous glucose production in PPARγ2 mice, we performed hyperinsulinemic euglycemic clamp experiments. Basal glucose production in PPARγ2 mice was decreased by 22% as compared with that in LacZ mice, whereas insulin's ability to suppress endogenous glucose production was severely blunted in PPARγ2 mice (Fig. 2F). In addition, glucose infusion rates in PPARγ2 mice were markedly increased (Fig. 2G). Thus, hepatic PPARγ2 expression improved insulin sensitivity in the periphery and decreased glucose output from the liver despite hepatic insulin resistance.

Serum free–fatty-acid (FFA) levels were markedly increased in PPARγ2 mice (fig. S4A), suggesting that hepatic PPARγ2 expression promotes hydrolysis of triglycerides stored in adipose tissues. Increased expression levels of the uncoupling protein (UCP)–1 (*15*), PGC1α (*16*), and hormone-sensitive lipase (*17*) in BAT (fig. S4B) and WAT (fig. S4C) indicate high tonus of the sympathetic nerves innervating these adipose tissues. In addition, the administration of bupranorol, a pan–β-adrenergic blocker (*18*), decreased serum FFA in PPARγ2 mice but had no effect in LacZ mice (fig. S4D), confirming that the β-adrenergic nerve function enhances lipolysis in adipose tissues of PPARγ2 mice.

To examine whether afferent nerves originating in the liver mediate the remote effects, we dissected the hepatic branch of the vagus nerve. Seven days after selective hepatic vagotomy (HV), we administered recombinant adenovirus encoding LacZ or PPARγ2 to mice. Hepatic PPARγ2 expression similarly altered liver weights, hepatic triglyceride content, and PEPCK expression in mice subjected to HV and sham operation (SO) (Table 1). In contrast, selective HV completely blocked the decreases in WAT weights and brown adipocyte size as well as the increases in serum FFA, resting oxygen consumption, and WAT UCP1 expression in PPARγ2 mice (Table 1), indicating that the hepatic vagus mediates the remote effects of hepatic PPARγ2 expression.

HV involves dissection of both afferent and efferent vagal branches innervating the liver. To determine whether the remote effects of hepatic PPARγ2 expression are mediated by the afferent vagus, we applied a specific afferent neurotoxin, capsaicin, to the hepatic branch of the vagus of diet-induced obese male Sprague-Dawley (SD) rats. Seven days after perivagal application of capsaicin or vehicle, we administered recombinant adenovirus encoding LacZ or PPARγ2. Expression of calcitonin gene–related peptide, a sensory neuropeptide, was markedly decreased in the capsaicin-treated vagal nerve, whereas immunoreactivity for S100 proteins was similar in vehicle- and capsaicin-treated nerves (fig. S5A). Furthermore, transmission electron microscopic analyses (fig. S5B) revealed selective degradation of unmyelinated fibers in the vagal hepatic branch. In addition, application of capsaicin to this branch did not affect the esophageal branch of the posterior vagal trunk (fig. S5). These observations indicate selective deafferentation of the hepatic branch of the vagus. Under these conditions, perivagal capsaicin treatment completely blocked the hepatic PPARγ2 expression–induced decrease in WAT weight (Table 1). When taken together, these findings strongly suggest that afferent vagal nerve ac-

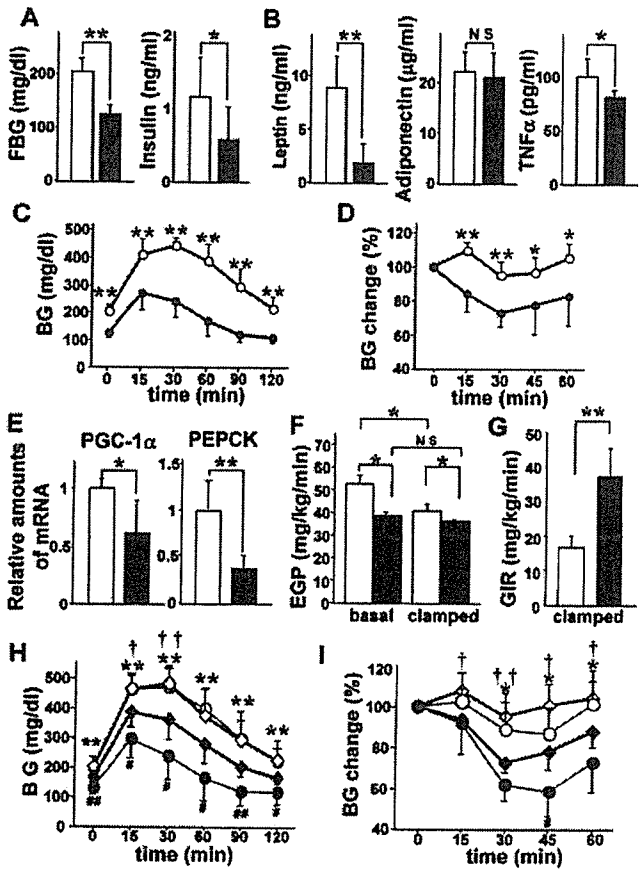

Fig. 2. Hepatic PPARγ2 expression improves peripheral insulin resistance. Fasting blood glucose (FBG) and serum insulin (**A**) and adipocytokines (**B**) were measured in LacZ mice (white bars) and PPARγ2 mice (black bars) on day 7 after adenoviral administration. These serum parameters were measured after a 10-hour fast. (**C** and **D**) LacZ mice (open circles) and PPARγ2 mice (solid circles) were subjected to glucose tolerance (C) and insulin tolerance (D) tests. BG, blood glucose. (**E**) Relative amounts of PGC-1α and PEPCK mRNA in the liver were measured by quantitative reverse transcriptase polymerase chain reaction. (**F** and **G**) Metabolic variables during hyperinsulinemic euglycemic clamp. Endogenous glucose production (EGP) in basal and clamped states (F) and rates of glucose infusion (GIR) were required to maintain euglycemia during the clamp study (G). Experiments in (A) to (G) were performed on day 7 after adenoviral administration. In (A), (B), and (E) to (G), white and black bars indicate results from LacZ mice and PPARγ2 mice, respectively. Significance as compared to LacZ mice is indicated (**$P < 0.01$ and *$P < 0.05$) by an unpaired t test. NS, not significant. (**H** and **I**) HV or SO was performed 7 days before the administration of LacZ or PPARγ2 adenovirus. Mice were subjected to glucose tolerance (H) and insulin tolerance (I) tests on day 7 after adenoviral administration. Open and solid circles indicate SO LacZ mice and SO PPARγ2 mice, respectively. Open and solid diamonds indicate HV LacZ mice and HV PPARγ2 mice, respectively. Data are presented as mean ± SD. **($P < 0.01$) and *($P < 0.05$) indicate significance in SO LacZ mice versus SO PPARγ2 mice, ††($P < 0.01$) and †($P < 0.05$) indicate significance in HV LacZ mice versus HV PPARγ2 mice, and ##($P < 0.01$) and #($P < 0.05$) indicate significance in HV PPARγ2 mice versus SO PPARγ2 mice, by unpaired t tests.

tivation originating in the liver mediates the remote effects of hepatic PPARγ2 expression on peripheral lipolysis.

We next examined the effects of HV on glucose (Fig. 2H) and insulin (Fig. 2I) tolerance test results in PPARγ2 mice. In SO mice, glucose tolerance and insulin sensitivity were improved by hepatic PPARγ2 expression, but these improvements were partially suppressed by hepatic branch vagotomy. These findings suggest that hepatic PPARγ2 expression improved glucose tolerance and systemic insulin sensitivity via both improved peripheral insulin sensitivity and decreased hepatic glucose output; the former requires afferent vagal and efferent sympathetic nerves, whereas the latter does not.

Next, to determine whether the neuronal system, consisting of afferent vagal and efferent sympathetic nerves, functions in the physiological setting of enhanced endogenous PPARγ2 expression in the liver, we examined the effects of an antidiabetic thiazolidinedione (TZD, a PPARγ agonist) using db/db mice, which are a murine model of genetic obesity and diabetes. In db/db mice, endogenous expression of PPARγ2, at both the mRNA (Fig. 3A) and the protein (fig. S6A) levels, is markedly enhanced in the liver. To eliminate the secondary effects of body weight changes, troglitazone, a TZD derivative, was given to db/db mice for 2 days, followed by an evaluation of acute effects. The TZD administration did not alter body weights (Fig. 3B) but did increase resting oxygen consumption (Fig. 3C) and UCP1 expression in BAT (Fig. 3D) and WAT (Fig. 3E), suggesting activation of sympathetic nerves to BAT and WAT. Dissection of the hepatic branch of the vagus 7 days before TZD administration reversed the increases in resting oxygen consumption (Fig. 3C) as well as UCP1 expression in BAT (Fig. 3D) and WAT (Fig. 3E). These findings indicate that the neuronal pathway originating in the liver is also involved in the acute systemic effects of TZDs, under conditions in which hepatic PPARγ expression is upregulated, such as in obese subjects.

To further examine whether endogenous PPARγ in the liver affects energy metabolism, we knocked down hepatic PPARγ in db/db mice. Administration of recombinant adenovirus expressing short hairpin RNA for PPARγ (*19*) 7 days before TZD treatment substantially decreased endogenous PPARγ expression in the liver (fig. S6B) as well as hepatic triglyceride content (fig. S6C) and sterol regulatory element binding protein–1c expression (fig. S6D), indicating functional knockdown of hepatic PPARγ (*20*). Under these conditions, TZD-enhanced energy expenditure was partially but significantly suppressed (fig. S6E). Thus, endogenous PPARγ in the liver regulates acute energy metabolism in vivo. TZD treatment reportedly alleviates insulin resistance in adipose-tissue–ablated mice (*10*) and adipose-specific-PPARγ–deficient mice (*21*), which may involve the aforementioned hepatic-PPARγ–induced neuronal activation in addition to a muscle PPARγ contribution (*22*).

We have shown that a neuronal pathway, consisting of the afferent vagus from the liver and efferent sympathetic nerves to adipose tissues, is involved in the regulation of energy expenditure, systemic insulin sensitivity, glucose metabolism, and fat distribution between the liver and the periphery. Because hepatic PPARγ expression is physiologically associated with obesity, the liver may convey information regarding excess energy balance to the CNS via the afferent vagus. This neuronal system may underlie chronic adaptive thermogenesis, resulting in protection against metabolic perturbation induced by excessive energy storage. There are two avenues of communication between the

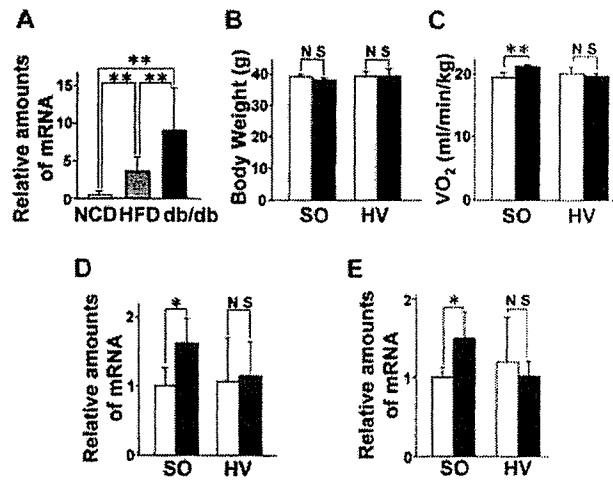

Fig. 3. HV inhibits TZD-enhanced energy expenditure in obese mice. (**A**) Relative amounts of PPARγ2 mRNA in the livers of normal chow diet–fed (NCD) C57BL/6 mice, high-fat diet–fed (HFD) C57BL/6 mice, and normal chow diet–fed db/db (db/db) mice. (**B** to **E**) db/db mice were subjected to HV or SO 7 days before the 2-day administration of TZD (black bars) or vehicle (white bars), after which body weights (B) and resting oxygen consumptions (C) were measured. Relative amounts of UCP1 mRNA in BAT (D) and epididymal fat tissue (E) from mice fed ad libitum. Data are presented as mean ± SD. Significance as compared to control mice is indicated (**$P < 0.01$ and *$P < 0.05$) by an unpaired t test. NS, not significant.

Table 1. Afferent vagal activation from the liver is involved in remote effects of hepatic PPARγ2 expression. (Upper section) Mice were subjected to HV or SO 7 days before administration of LacZ or PPARγ2 adenovirus. Resting oxygen consumption (VO_2) was measured on day 3 after adenoviral injection. Mice were killed after a 10-hour fast on day 7 after adenoviral injection. (Lower section) Male SD rats with high-fat diet–induced obesity were subjected to application of capsaicin or vehicle to the vagal hepatic branch 7 days before administration of LacZ or PPARγ2 adenovirus. Seven days after adenoviral administration, epididymal fat weights were determined. Significance as compared to LacZ mice is indicated (P values) by an unpaired t test. LW, liver weight; HTG, hepatic TG content; P, PEPCK; CD, cell diameter; NS, not significant.

	SO			HV		
	LacZ	PPARγ2	P	LacZ	PPARγ2	P
LW (g)	1.11 ± 0.13	2.30 ± 0.39	<0.001	1.12 ± 0.07	2.07 ± 0.32	<0.001
HTG (mg/g tissue)	78.71 ± 46.50	171.26 ± 43.90	0.008	62.02 ± 24.92	215.09 ± 75.78	<0.001
P mRNA (liver)	1.00 ± 0.21	0.50 ± 0.17	0.003	1.356 ± 0.460	0.54 ± 0.22	0.002
WAT weight (g)	1.13 ± 0.13	0.85 ± 0.14	<0.001	1.04 ± 0.26	1.06 ± 0.19	NS
BAT CD (μm)	11.55 ± 4.45	7.69 ± 2.09	<0.001	10.63 ± 3.38	10.55 ± 3.93	NS
FFA (μEq/l)	556.14 ± 87.33	860.47 ± 206.04	0.005	533.14 ± 59.50	558.38 ± 151.58	NS
VO_2 (ml/min/kg)	30.25 ± 2.38	34.38 ± 3.03	0.015	32.73 ± 4.54	31.98 ± 4.05	NS
UCP1 mRNA (WAT)	1.00 ± 0.24	2.36 ± 0.77	0.019	2.05 ± 0.64	1.82 ± 1.15	NS
	Vehicle			Capsaicin		
WAT weight (g)	8.95 ± 0.99	7.06 ± 1.32	0.024	8.70 ± 1.14	8.85 ± 1.71	NS

brain and other tissues: humoral factors and neuronal pathways. Leptin, a humoral factor from adipocytes, is a mediator of metabolic information from adipose tissue to the hypothalamus (*2*). In addition, circulating nutrients reportedly affect food intake and alter hepatic glucose production via the efferent vagal pathway (*23*, *24*). An afferent vagal signal originating in the liver is likely to be another metabolic information pathway. In this way, the brain may integrate information obtained from several tissues and organs via both humoral and neuronal pathways. When the brain receives information regarding excess energy storage, the sympathetic nervous system is activated to enhance energy expenditure and lipolysis, thereby maintaining energy homeostasis. Disturbance of the control system is implicated in the development of the metabolic syndrome (*25*). Targeting of this neuronal pathway is a potential therapeutic strategy for treating the metabolic syndrome.

References and Notes

1. J. S. Flier, *Cell* **116**, 337 (2004).
2. J. M. Friedman, J. L. Halaas, *Nature* **395**, 763 (1998).
3. Y. Minokoshi, C. R. Kahn, B. B. Kahn, *J. Biol. Chem.* **278**, 33609 (2003).
4. T. Kitamura, C. R. Kahn, D. Accili, *Annu. Rev. Physiol.* **65**, 313 (2003).
5. J. An *et al.*, *Nat. Med.* **10**, 268 (2004).
6. T. Yamada *et al.*, *Cell Metab.* **3**, 223 (2006).
7. O. Gavrilova *et al.*, *J. Biol. Chem.* **278**, 34268 (2003).
8. V. Bocher, I. Pineda-Torra, J. C. Fruchart, B. Staels, *Ann. N.Y. Acad. Sci.* **967**, 7 (2002).
9. L. Fajas *et al.*, *J. Biol. Chem.* **272**, 18779 (1997).
10. C. F. Burant *et al.*, *J. Clin. Invest.* **100**, 2900 (1997).
11. L. Chao *et al.*, *J. Clin. Invest.* **106**, 1221 (2000).
12. R. Rahimian *et al.*, *Mol. Cell. Biochem.* **224**, 29 (2001).
13. K. Matsusue *et al.*, *J. Clin. Invest.* **111**, 737 (2003).
14. Y. Ishigaki *et al.*, *Diabetes* **54**, 322 (2005).
15. I. Nagase *et al.*, *J. Clin. Invest.* **97**, 2898 (1996).
16. J. Gomez-Ambrosi, G. Fruhbeck, J. A. Martinez, *Mol. Cell. Endocrinol.* **176**, 85 (2001).
17. Y. Hatakeyama, Y. Sakata, S. Takakura, T. Manda, S. Mutoh, *Am. J. Physiol. Regul. Integr. Comp. Physiol.* **287**, R336 (2004).
18. A. Wellstein, D. Palm, G. G. Belz, *J. Cardiovasc. Pharmacol.* **8** (suppl. 11), S36 (1986).
19. T. Hosono *et al.*, *Gene* **348**, 157 (2005).
20. S. Herzig *et al.*, *Nature* **426**, 190 (2003).
21. W. He *et al.*, *Proc. Natl. Acad. Sci. U.S.A.* **100**, 15712 (2003).
22. A. L. Hevener *et al.*, *Nat. Med.* **9**, 1491 (2003).
23. A. Pocai, S. Obici, G. J. Schwartz, L. Rossetti, *Cell Metab.* **1**, 53 (2005).
24. T. K. Lam *et al.*, *Nat. Med.* **11**, 320 (2005).
25. M. W. Schwartz, D. Porte Jr., *Science* **307**, 375 (2005).

26. We thank M. Kaji, T. Takai, Y. Sato, H. Yawo, T. Hashikawa, M. Kanzaki, Y. Minokoshi, and M. Tominaga for advice and discussions. Supported by grants-in-aid from the Ministry of Education, Science, Sports, and Culture of Japan (H.K.), a grant-in-aid from the Ministry of Health, Labor, and Welfare of Japan (Y.O.), and the 21st Century Center of Excellence Programs (H.K. and Y.O.).

Supporting Online Material

www.sciencemag.org/cgi/content/full/312/5780/1656/DC1
Materials and Methods
SOM Text
Figs. S1 to S6
Table S1
References

9 February 2006; accepted 8 May 2006
10.1126/science.1126010

Synaptic Amplifier of Inflammatory Pain in the Spinal Dorsal Horn

Hiroshi Ikeda,* Johanna Stark, Harald Fischer, Matthias Wagner, Ruth Drdla, Tino Jäger, Jürgen Sandkühler†

Inflammation and trauma lead to enhanced pain sensitivity (hyperalgesia), which is in part due to altered sensory processing in the spinal cord. The synaptic hypothesis of hyperalgesia, which postulates that hyperalgesia is induced by the activity-dependent long-term potentiation (LTP) in the spinal cord, has been challenged, because in previous studies of pain pathways, LTP was experimentally induced by nerve stimulation at high frequencies (~100 hertz). This does not, however, resemble the real low-frequency afferent barrage that occurs during inflammation. We identified a synaptic amplifier at the origin of an ascending pain pathway that is switched-on by low-level activity in nociceptive nerve fibers. This model integrates known signal transduction pathways of hyperalgesia without contradiction.

Inflammation of peripheral tissues causes spontaneous pain and hyperalgesia. Amplification of pain-related information in the spinal dorsal horn lamina I contributes to inflammatory pain (*1*–*6*). Inflammation causes release of neuromodulators, including substance P and glutamate in spinal dorsal horn (*7*, *8*), potentially leading to Ca^{2+}-dependent LTP. In all previous studies, spinal LTP was induced by brief (1 s), high-frequency (100 Hz) burstlike stimulation (HFS) of afferent nerve fibers. High-frequency bursts do not, however, resemble the continuous low-frequency afferent barrage that occurs during inflammation. Low-frequency presynaptic activity normally fails to induce LTP but rather induces synaptic long-term depression (LTD) (*9*). The LTP model of inflammatory hyperalgesia thus may be questioned. Here, we evaluated the effect of low-frequency afferent barrage on synaptic transmission in ascending pain pathways and asked if synaptic plasticity is differentially induced in distinct ascending pain tracts. We labeled lamina I projection neurons by retrograde fluorescent marker DiI (1,1′-dioctadecyl-3,3,3′,3′-tetramethylindocarbocyanine perchlorate), injected into either of two major projection areas of spinal lamina I neurons: the parabrachial (PB) area or the periaqueductal gray (PAG) (*10*, *11*) (Fig. 1, A and B). To circumvent confounding developmental factors, we used only juvenile or adult rats in this study. Transverse spinal cord slices with long dorsal roots attached were prepared 3 to 4 days after DiI injections to allow whole-cell recordings from identified projection neurons in 21- to 28-day-old rats (*10*). In the presence of tetrodotoxin, bath application of substance P (2 μM) induced transient inward currents in 21 out of 27 spino-PB and in 9 out of 12 spino-PAG neurons (Fig. 1C), confirming the expression of functional neurokinin 1 receptors (NK1Rs). Spinal release of substance P following electrical stimulation of primary afferents at C-fiber strength was assessed by the internalization of NK1R in lamina I neurons. HFS parameters (100-Hz bursts) similar to all previously used conditioning stimulation protocols to induce classical LTP in pain pathways, or low-frequency stimulation (LFS, 2 Hz), was used. Both types of stimulation elicited substantial NK1R internalization in 89 ± 1% and in 78 ± 4% of 150 neurons evaluated in three rats per group (Fig. 1D). We then used these stimulation protocols for conditioning.

Conditioning HFS induces LTP at synapses between C-fibers and lamina I neurons that project to the PB (*12*). We confirmed these results by showing LTP of monosynaptically evoked excitatory postsynaptic currents (EPSCs) to 172 ± 15% of the control value at 30 min after conditioning ($n = 8$) (Fig. 2A). However, conditioning electrical stimulation within the typical frequency band of C-fibers during inflammation (2 Hz) (*13*) did not change synaptic strength in any of the spino-PB neurons tested (108 ± 19% of control, $n = 7$) (Fig. 2C). LFS, however, did modify synaptic strength in spinal lamina I neurons with a projection to the PAG. In all spino-PAG neurons tested, LFS induced a robust LTP of monosynaptic C-fiber–evoked EPSCs [to 262 ± 30% of the control value at 30 min after stimulation ($n = 18$) and to 346 ± 33% at 60 min ($n = 8$)] (Fig. 2D). In all seven lamina I neurons with a projection to the PAG, conditioning stimulation at high frequency was ineffective (98 ± 10%, $n = 7$) (Fig. 2B). Monosynaptic, A-fiber–evoked

Department of Neurophysiology, Center for Brain Research, Medical University of Vienna, Vienna, Austria.

*Present address: Department of Human and Artificial Intelligence Systems, University of Fukui, 3-9-1 Bunkyo, Fukui 910-8507, Japan.

†To whom correspondence should be addressed. E-mail: juergen.sandkuehler@meduniwien.ac.at

FEBS Letters 580 (2006) 5635–5640

WFS1 protein modulates the free Ca^{2+} concentration in the endoplasmic reticulum

Daisuke Takei[a], Hisamitsu Ishihara[a,*], Suguru Yamaguchi[a], Takahiro Yamada[a], Akira Tamura[a], Hideki Katagiri[b], Yoshio Maruyama[c], Yoshitomo Oka[a]

[a] *Division of Molecular Metabolism and Diabetes, Tohoku University Graduate School of Medicine, 2-1 Seiryo-machi, Aoba-ku, Sendai 980-8575, Japan*
[b] *Division of Advanced Therapeutics for Metabolic Diseases, Tohoku University Graduate School of Medicine, Sendai 980-8575, Japan*
[c] *Department of Physiology, Tohoku University Graduate School of Medicine, Sendai 980-8575, Japan*

Received 29 June 2006; revised 20 August 2006; accepted 5 September 2006

Available online 15 September 2006

Edited by Felix Wieland

Abstract **The *WFS1* gene, encoding an endoplasmic reticulum (ER) membrane glycoprotein, is mutated in Wolfram syndrome characterized by diabetes mellitus and optic atrophy. Herein, Ca^{2+} dynamics were examined in WFS1-knockdown and -overexpressing HEK293 cells. Studies using ER-targeted Ca^{2+}-sensitive photoprotein aequorin demonstrated WFS1 protein to positively modulate ER Ca^{2+} levels by increasing the rate of Ca^{2+} uptake. Furthermore, Ca^{2+} imaging with Fura-2 showed the magnitude of the store-operated Ca^{2+} entry to parallel WFS1 expression levels. These data indicate that WFS1 protein participates in the regulation of cellular Ca^{2+} homeostasis, at least partly, by modulating the filling state of the ER Ca^{2+} store.**

Keywords: Wolfram syndrome; WFS1; Endoplasmic reticulum; Cellular Ca^{2+} homeostasis

1. Introduction

Ca^{2+} signals control various biological functions [1] and, thus, impaired cellular Ca^{2+} homeostasis underlies a wide variety of human diseases [2]. The endoplasmic reticulum (ER), which constitutes the main intracellular Ca^{2+} store, plays a central role in Ca^{2+} homeostasis. The ER releases Ca^{2+} in response to external stimuli through the inositol 1,4,5-trisphosphate receptor and by a process of Ca^{2+}-induced Ca^{2+} release [3]. In addition, changes in intraluminal Ca^{2+} concentrations of the ER ($[Ca^{2+}]_{er}$) regulate Ca^{2+} influx through the plasma membrane, a process known as store-operated Ca^{2+} (SOC) entry [4]. Furthermore, Ca^{2+} in the ER also plays important roles in the functions, such as protein folding, of this organelle. The activities of several ERresident chaperone proteins are Ca^{2+}-dependent. Thus, a decrease in $[Ca^{2+}]_{er}$ causes misfolding of ER resident proteins, accumulation of which triggers the so-called ER stress response in the cell, leading to apoptosis in severe cases [5].

Wolfram syndrome, an autosomal recessive disorder characterized by juvenile-onset diabetes mellitus and optic atrophy [6], is caused by mutations in the *WFS1* gene [7,8]. WFS1 protein, also called wolframin, consisting of 890 amino acids, is a type II membrane protein with 9 putative transmembrane segments [9] and localizes in the ER [10]. Lack of distinct domain structures in WFS1 protein makes it difficult to identify its functions. We [11] and others [12] recently established mutant mice with a disrupted *wfs1* gene and found that these mice exhibited impaired glucose homeostasis. In *wfs1*-deficient β-cells, glucose-stimulated elevation of the cytosolic Ca^{2+} concentration ($[Ca^{2+}]_{cyt}$) was impaired [11], and the ER-stress response was persistently activated [13]. In addition, wolframin expression reportedly conferred cation channel activity and increased $[Ca^{2+}]_{cyt}$ levels in *Xenopus* oocytes [14]. These data suggested WFS1 protein to play a role in cellular Ca^{2+} homeostasis and regulation of ER functions. Herein, by analyzing WFS1-knockdown and -overexpressing HEK293 cells, we show that WFS1 protein modulates $[Ca^{2+}]_{er}$ by positively regulating the ER Ca^{2+} uptake, which is associated with changes in the $[Ca^{2+}]_{cyt}$ response evoked by Ca^{2+} store depletion.

2. Materials and methods

2.1. Generation of WFS1-knockdown and -overexpressing HEK293 cell clones

The human H1 promoter containing two *tet* operator sequences (Fig. 1A) was generated by PCR. A DNA fragment encoding short hairpin RNA (shRNA) against human *WFS1* 2254–2274 nt (GAGGAGCTCTGTCGCCTTAAG) were generated by PCR. HEK293-TRex cells (Invitrogen) were transfected with the shRNA expressing plasmid and selected against hygromycin (200 μg/ml). Two independent clones were analyzed but data obtained with clone #36 which had the highest knockdown efficiency are presented. To establish WFS1-overexpressing clones, wild-type human WFS1 cDNA was subcloned into a pTRE-Tight vector (Clontech). HEK293-rtTA cells (Clontech) were then transfected with the pTRE-Tight derivative. Two independent clones were analyzed but data obtained with clone #31 with the tightest inducibility by doxycycline (Dox, 2 μg/ml) are presented. It should be noted that WFS1-knockdown and -overexpressing cells are based on different HEK293 cell transformants,

*Corresponding author. Fax: +81 22 717 7612.
E-mail addresses: hisamitsu-ishihara@mail.tains.tohoku.ac.jp, ishihara-tky@umin.ac.jp (H. Ishihara).

Abbreviations: $[Ca^{2+}]_{cyt}$, cytosolic Ca^{2+} concentration; $[Ca^{2+}]_{er}$, ER Ca^{2+} concentration; $[Ca^{2+}]_{mt}$, mitochondrial Ca^{2+} concentration; CPA, cyclopiazonic acid; Dox, doxycycline; ER, endoplasmic reticulum; erAEQ, ER-targeted aequorin; SERCA, salco(endo)plasmic reticulum Ca^{2+} ATPase; shRNA, short hairpin RNA; SOC, store-operated Ca^{2+}; TG, thapsigargin

0014-5793/$32.00
doi:10.1016/j.febslet.2006.09.007

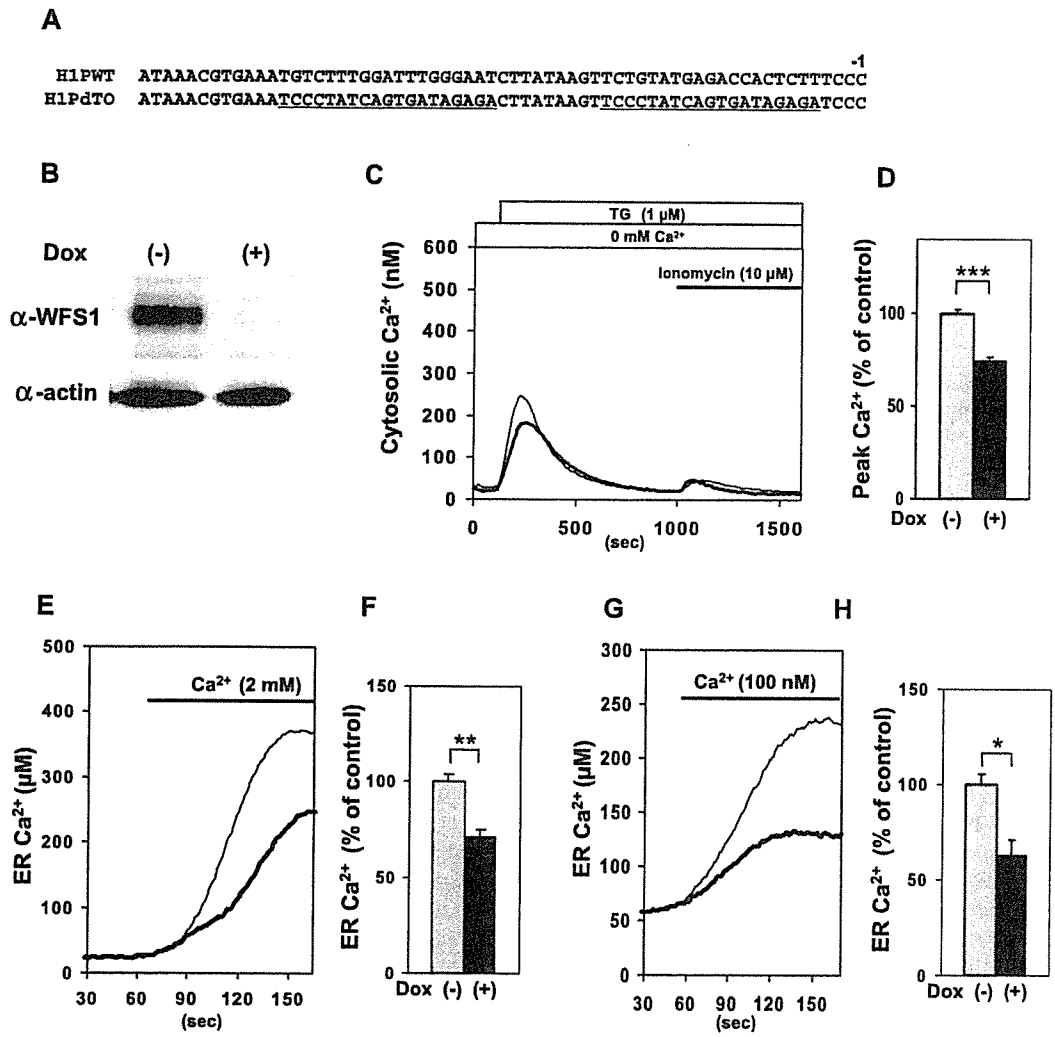

Fig. 1. Reduced ER Ca^{2+} concentrations in WFS1-knockdown cells. (A) A part of sequence of the modified human H1 promoter (H1PdTO) containing two *tet*-operator sequences (underlined) is aligned with the wild-type H1 promoter (H1PWT). (B) Expression of WFS1 protein was knocked down in HEK293 cells expressing shRNA against the *WFS1* transcript by treatment with Dox (2 μg/ml) for 3 days. (C) Cells loaded with Fura-2 were perfused in Ca^{2+}-free solution, and TG (1 μM) was then added, followed by ionomycin (10 μM). Small and comparable ionomycin-induced Ca^{2+} rises indicated that TG efficiency for emptying ER Ca^{2+} were similar between control and WFS1-knockdown cells. Traces are averages of 37 control (thin line) and 41 knockdown (thick line) cells from 3 experiments. (D) Peak amplitudes of TG-induced $[Ca^{2+}]_{cyt}$ were quantified. Gray bar, control cells ($n = 37$); Black bar, WFS1-knockdown cells ($n = 41$). (E) $[Ca^{2+}]_{er}$ in WFS1-knockdown cells measured using erAEQ. Cells transfected with an erAEQ plasmid were perfused with Ca^{2+}-free solution, followed by readdition of Ca^{2+}. Traces are representative of six perfusions each of control (thin line) and WFS1-knockdown (thick line) cells. (F) Plateau $[Ca^{2+}]_{er}$ levels in control (gray bar) and WFS1-knockdown (black bar) cells are compared ($n = 6$). (G) $[Ca^{2+}]_{er}$ measured with erAEQ in permeabilized cells. Traces are representative of four perfusions each of control (thin line) and WFS1-knockdown (thick line) cells. (H) Plateau $[Ca^{2+}]_{er}$ levels in permeabilized control (gray bar) and WFS1-knockdown (black bar) cells are compared ($n = 4$). $^{*}P < 0.05$, $^{**}P < 0.01$, $^{***}P < 0.001$.

and therefore control cells differed in WFS1-knockdown and -over-expressing experiments.

2.2. Immunodetection

HEK293 cell transformants treated with or without Dox were dissolved in 1× SDS-sample buffer. Cellular lysates were subjected to SDS–PAGE and were probed with rabbit anti-WFS1 [11], anti-actin or anti-salco(endo)plasmic reticulum Ca^{2+} ATPase (SERCA)-2 antibody (Sigma). Detection was accomplished with chemiluminescence (Amersham). HEK293 cell transformants were also fixed with 4% paraformaldehyde, permeabilized, and probed with anti-WFS1 antibody. For double staining, cells were incubated with 50 nM MitoTracker Red (Molecular Probes) for 30 min at 37 °C before fixation. The fluorescent signal was observed with an FV1000 microscope system (Olympus).

2.3. Aequorin measurement

We built our own luminescence measurement apparatus using a photomultiplier (H7360-1: Hamamatsu Photonics) and a photon counting board (M8784: Hamamatsu Photonics). For measurement of $[Ca^{2+}]_{er}$, cells seeded on coverslips and transfected with ER-targeted aequorin (erAEQ) cDNA [15] were incubated in Ca^{2+}-free solution containing 2 mM EGTA and 10 μM cyclopiazonic acid (CPA) to deplete ER Ca^{2+} and erAEQ was reconstituted with 5 μM *n*-coelenterazine (Biotium) for 60 min at 4 °C. Cells on coverslips were placed on the luminescence measurement apparatus and perfused at a flow rate of 1.5 ml/min of physiological salt solution. Experiments were terminated by lysing the cells with 100 μM digitonin in Ca^{2+}-rich solution. In some cases, cells were permeabilized with a 30 s treatment with 40 μM β-escin. Cells were first perfused with an intracellular type buffer containing 1 mM EGTA (without addition of $CaCl_2$), followed by a buffer

adjusted to approximately 100 nM free Ca^{2+} (140 mM KCl, 5 mM NaCl, 7 mM $MgSO_4$, 20 mM HEPES, pH 7.0, 10 mM ATP, 10.2 mM EGTA, 1.65 mM $CaCl_2$) at 37 °C. $[Ca^{2+}]_{mt}$ was measured according to a published method [16].

2.4. Ca^{2+} imaging using Fura-2 and Mn^{2+} quench analysis

Fluorescent images of single cells loaded with 1 μM Fura-2 acetoxymethyl ester were generated by alternate excitations at 340 and 380 nm every 10 s in physiological salt solution at 25–27 °C. $[Ca^{2+}]_{cyt}$ was calculated as reported previously [17]. For Mn^{2+} quench experiments [18], cells were perfused in Ca^{2+} free solution supplemented with thapsigargin (1 μM), followed by addition of Mn^{2+} (30 μM). Single-cell images (excitation 360 nm, emission 510 nm) were then captured.

2.5. Statistical analysis

Data are presented as means ± S.E. Differences between groups were assessed by Student's *t*-test for unpaired data.

3. Results and discussion

3.1. The free Ca^{2+} concentration in the ER is reduced in WFS1-knockdown cells

We generated WFS1-knockdown HEK293 cell clones in which WFS1 protein expression was suppressed by expressing short hairpin RNA (shRNA) against the *WFS1* transcript via a doxycycline (Dox)-inducible promoter (Fig. 1A). HEK293 cells were selected because they express WFS1 protein and lack voltage-dependent Ca^{2+} channels, simplifying data interpretation. As shown in Fig. 1B, Dox-treatment caused nearly 100% knockdown of WFS1 protein expression.

We first examined the effects of WFS1-deficiency on Ca^{2+} release from the ER induced by thapsigargin (TG), an inhibitor of salco(endo)plasmic reticulum Ca^{2+} ATPase (SERCA). When WFS1-knockdown cells were challenged with TG in the absence of extracellular Ca^{2+}, $[Ca^{2+}]_{cyt}$ elevation as measured with Fura-2 was blunted in comparison with that in control cells (Fig. 1C and D), suggesting ER Ca^{2+} content to be decreased in WFS1-knockdown cells. We, thus, directly measured $[Ca^{2+}]_{er}$ using ER-targeted aequorin (erAEQ) [15] in WFS1-knockdown cells. Knockdown of WFS1 expression was associated with a $[Ca^{2+}]_{er}$ decrease (Fig. 1E and F). To investigate whether reductions in $[Ca^{2+}]_{er}$ were direct WFS1 knockdown effects on the ER, we studied the $[Ca^{2+}]_{er}$ in WFS1-knockdown cells permeabilized with β-escin. Permeabilized cells were perfused with Ca^{2+}-free intracellular type buffer, which was switched to a buffer containing the Ca^{2+} concentration of approximately 100 nM and 10 mM ATP. The $[Ca^{2+}]_{er}$ were gradually increased with 35% lower plateaus in WFS1-knockdown than in control cells (Fig. 1G and H). These data indicated the effects of WFS1 knockdown on $[Ca^{2+}]_{er}$ to not be indirect, i.e. to not occur via the plasma membrane or cytosolic factors. Importantly, the initial rate of Ca^{2+} refilling was lower in WFS1-knockdown than in control cells (Fig. 1G; 1.88 ± 0.19 vs. 1.10 ± 0.22 μM/s for control ($n = 4$) and knockdown ($n = 4$) cells, $P < 0.05$), indicating involvement of WFS1 protein in Ca^{2+} uptake by the ER.

3.2. The Ca^{2+} concentration in the ER is increased in WFS1-overexpressing cells

We also generated HEK293 cell clones Dox-dependently overexpressing wild-type WFS1 protein. Dox-treatment induced high level expression of WFS1 protein with a reticular pattern typical for ER localization (Fig. 2A). Overexpressed WFS1 protein did not colocalize with a mitochondrial marker, MitoTracker Red (Fig. 2B). When $[Ca^{2+}]_{er}$ were measured using erAEQ, $[Ca^{2+}]_{er}$ were significantly higher in WFS1-overexpressing than in control cells (Fig. 2C and D). Analysis in permeabilized cells revealed WFS1-overxpression to result in higher plateau $[Ca^{2+}]_{er}$ levels (Fig. 2E and F) and greater initial Ca^{2+} uptake rates (Fig. 2E; 1.42 ± 0.17 vs. 2.37 ± 0.21 μM/s for control ($n = 7$) and overexpressing ($n = 7$) cells, $P < 0.01$), indicating WFS1-protein to activate Ca^{2+} uptake by the ER. To gain insight into the increased $[Ca^{2+}]_{er}$ associated with WFS1 overexpression, we next studied Ca^{2+} refilling of the ER in the presence of cyclopiazonic acid (CPA), another SERCA inhibitor (Fig. 2G). Refilling of Ca^{2+} in intact WFS1-overexpressing cells was inhibited as potently as that in control cells, indicating Ca^{2+} uptake to also be mediated by the SERCA Ca^{2+} pump in WFS1-overexpressing cells. We then studied expression of SERCA2, a major isoform of SERCA in HEK293 cells, and found no difference in its expression between WFS1-overexpressing and control cells (Fig. 2H). These results suggest WFS1 protein to modulate intrinsic activity of the SERCA Ca^{2+} pump. Future studies should be designed to elucidate molecular mechanisms of interaction between SERCA and WFS1 proteins.

3.3. SOC entry is modulated in WFS1-knockdown and -overexpressing cells

ER Ca^{2+} homeostasis affects cytosolic Ca^{2+} signaling [4]. We thus studied $[Ca^{2+}]_{cyt}$ dynamics after ER Ca^{2+} depletion in WFS1-knockdown and -overexpressing cells. When cells were treated with TG in the absence of extracellular Ca^{2+}, emptying the ER Ca^{2+} store, and then readded with Ca^{2+}, $[Ca^{2+}]_{cyt}$ responses were lower in WFS1-knockdown (Fig. 3A and B) and higher in WFS1-overexpressing (Fig. 3C and D) cells, as compared to those in control cells. The muscarinic agonist carbachol is known to induce Ca^{2+} release from the ER and subsequent Ca^{2+} influx through the plasma membrane. Carbachol-induced increases in $[Ca^{2+}]_{cyt}$ in the presence of extracellular Ca^{2+}, especially during the declining phase of the Ca^{2+} transient, were also greater in WFS1-overexpressing cells (Fig. 3E).

Modulation of Ca^{2+} influx through SOC channels could be responsible for the observed Ca^{2+} responses after store depletion. Thus, Ca^{2+} influx after depletion of the ER Ca^{2+} store was directly monitored with a Mn^{2+} quench technique [18]. We found the initial Mn^{2+} quenching rates to be slower in WFS1-knockdown cells (Fig. 3F; 100 ± 3.12 vs. 70.48 ± 3.33 (arbitrary units) for control ($n = 96$) and knockdown ($n = 109$) cells, $P < 0.001$) and faster in WFS1-overexpressing cells (traces not shown, 100 ± 5.73 vs. 136.48 ± 7.64 for control ($n = 124$) and overexpressing ($n = 127$) cells, $P < 0.01$) than in control cells.

Since the uptake of Ca^{2+} by mitochondria modulates $[Ca^{2+}]_{cyt}$ [19], changes in mitochondrial Ca^{2+} uptake could theoretically be another factor affecting the $[Ca^{2+}]_{cyt}$ response in WFS1-knockdown and -overexpressing cells. Mitochondrial Ca^{2+} concentrations ($[Ca^{2+}]_{mt}$) were, thus, studied using mitochondrial-targeted aequorin upon Ca^{2+} readdition after CPA-induced store depletion. $[Ca^{2+}]_{mt}$ was essentially unaltered in WFS1-knockdown cells (Fig. 3G), although the peak $[Ca^{2+}]_{mt}$ was slightly decreased (1.26 ± 0.07 vs. 1.04 ± 0.04 μM for

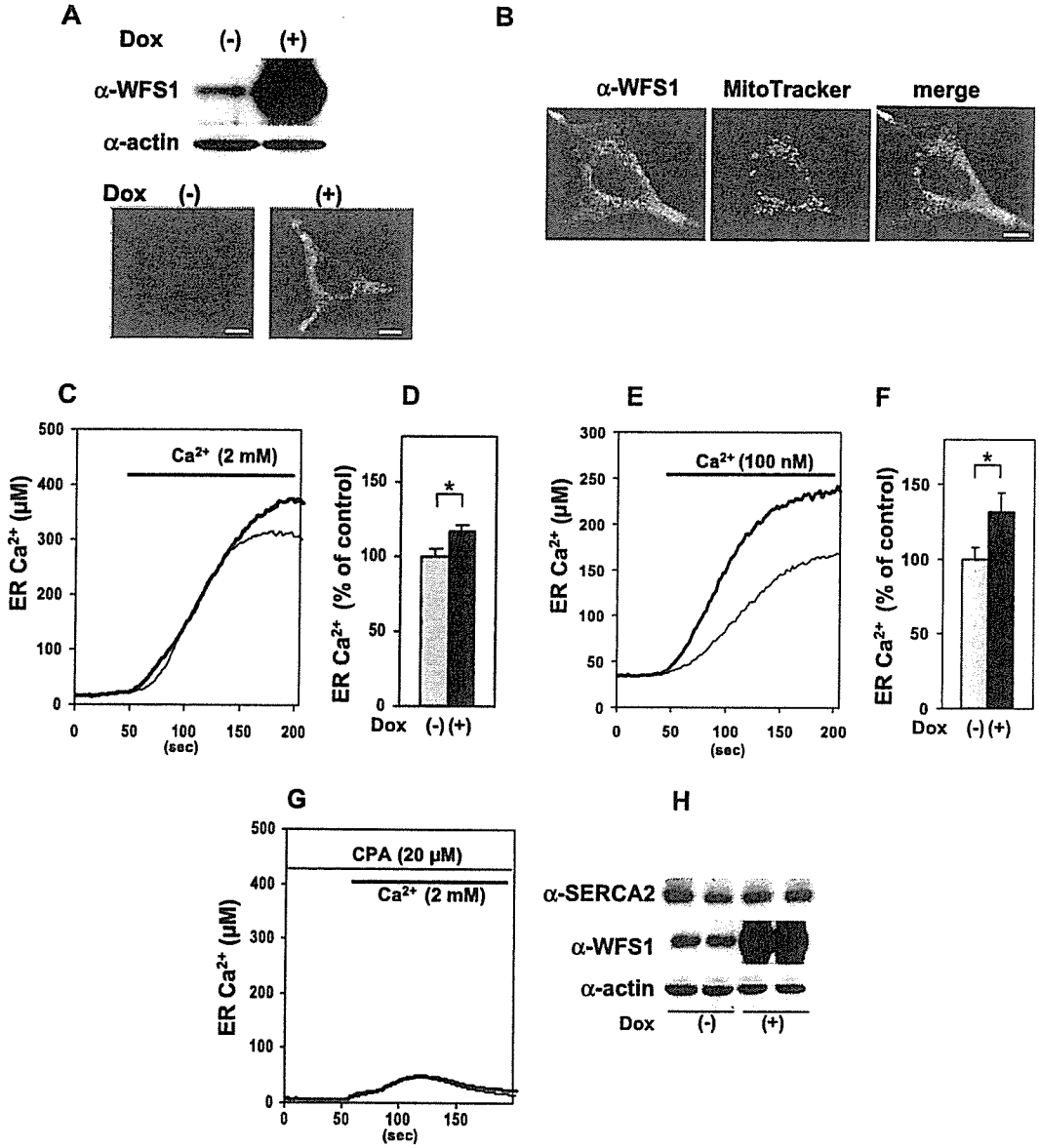

Fig. 2. Increased ER Ca^{2+} concentrations in WFS1-overexpressing cells. (A) Overexpression of WFS1 was induced by treatment with Dox (2 μg/ml) for three days. Note that our WFS1 antibody detected endogenous WFS1 on Western blotting but was not sensitive enough to detect it on immunohistochemistry in HEK293 cells. Bars, 4 μm. (B) WFS1-overexpressing cells were incubated with 50 nM MitoTracker Red before fixation and stained using an anti-WFS1-antibody. Bar, 4 μm. (C) $[Ca^{2+}]_{er}$ in WFS1-overexpressing cells. Traces are representative of 10 perfusions each of control (thin line) and WFS1-overexpressing (thick line) cells. (D) Plateau $[Ca^{2+}]_{er}$ levels in control (gray bar) and WFS1-overexpressing (black bar) cells are compared ($n = 10$). (E) $[Ca^{2+}]_{er}$ in permeabilized WFS1-overexpressing cells. Traces are representative of seven perfusions each of control (thin line) and WFS1-overexpressing (thick line) cells. (F) Plateau $[Ca^{2+}]_{er}$ levels in permeabilized control (gray bar) and WFS1-overexpressing (black bar) cells are compared ($n = 7$). (G) $[Ca^{2+}]_{er}$ measured in intact control (thin line) and WFS1-overexpressing (thick line) cells in the presence of cyclopiazonic acid (CPA). Traces are representative of three perfusions. (H) Immunoblot of SERCA2 in WFS1-overexpressing cells. The blot shown is representative of three independent experiments. $^*P < 0.05$.

control ($n = 7$) and knockdown ($n = 7$) cells, $P < 0.05$). Thus, the decrease in the $[Ca^{2+}]_{cyt}$ response in WFS1-knockdown cells was not due to an increase in mitochondrial Ca^{2+} uptake. Conversely, in WFS1-overexpressing cells, $[Ca^{2+}]_{mt}$ upon Ca^{2+} readdition was increased (Fig. 3H; 1.36 ± 0.05 vs. 1.76 ± 0.04 μM for control ($n = 7$) and overexpressing ($n = 7$) cells, $P < 0.001$), excluding the possibility of the enhanced $[Ca^{2+}]_{cyt}$ response being due to reduced Ca^{2+} uptake by mitochondria. Taken together, these data indicated altered $[Ca^{2+}]_{cyt}$ responses after depletion of ER Ca^{2+} stores in WFS1-knockdown and -overexpressing cells to be not due to changes in mitochondrial Ca^{2+} uptake but due to changes in SOC entry.

Decreased SOC entry associated with reduced ER Ca^{2+} levels was previously reported in cells overexpressing the proapoptotic protein Bcl-2 [19,20] and in cells expressing presenilin mutants linked to familial Alzheimer's disease [21]. It was suggested that a reduction in $[Ca^{2+}]_{er}$ levels decreased SOC influx by an adaptive downregulation of the pathway

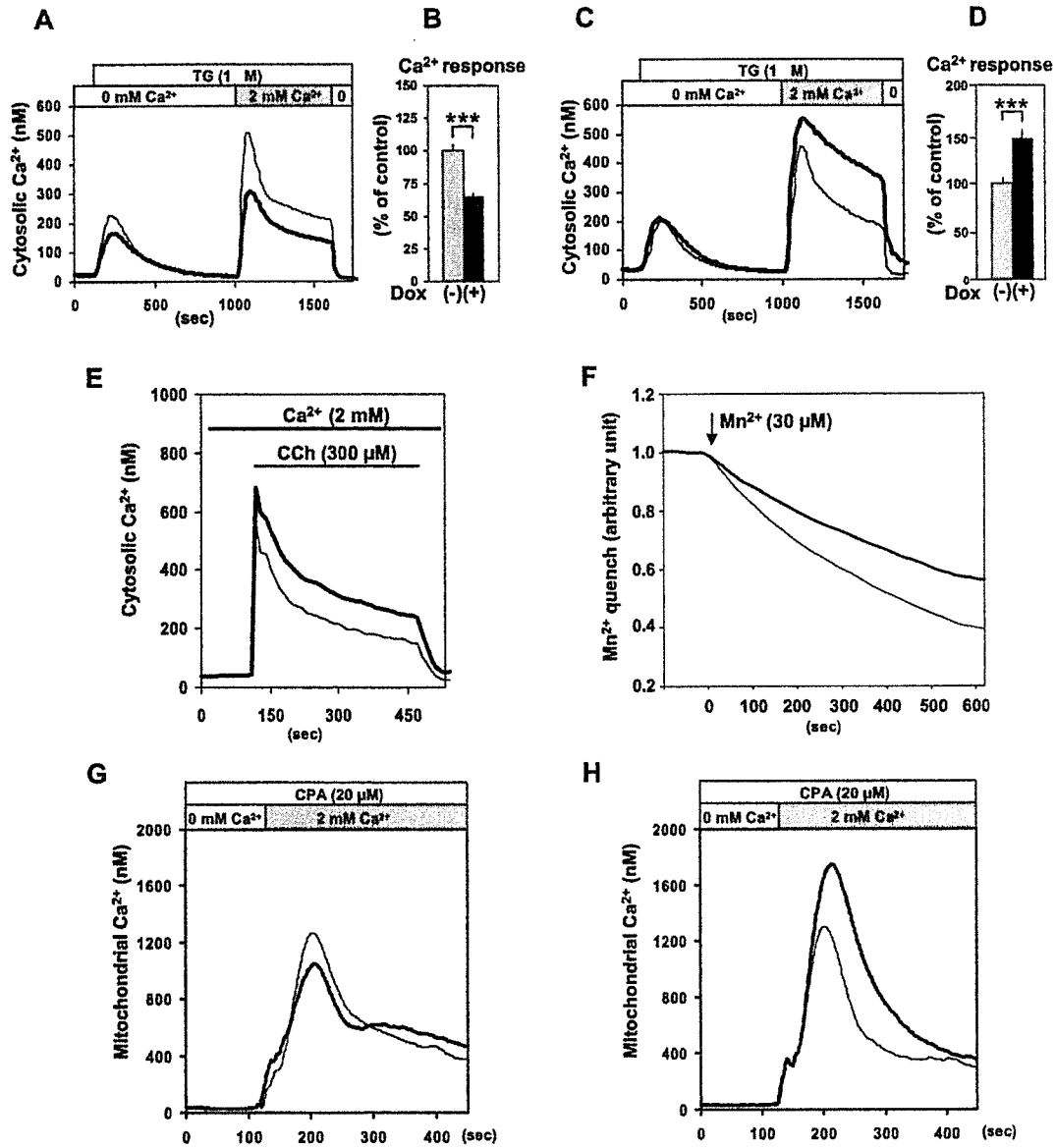

Fig. 3. Modulation of SOC entry in WFS1-knockdown and -overexpressing cells. (A) $[Ca^{2+}]_{cyt}$ responses to Ca^{2+} readdition after Ca^{2+} store depletion was analyzed with Fura-2 in control (thin line) and WFS1-knockdown (thick line) cells. Traces are averages of 62 control and 64 WFS1-knockdown cells from four experiments. (B) Areas under the curves (AUCs), in response to Ca^{2+} readdition in (A), were quantified. Gray bar, control cells ($n = 62$); Black bar, WFS1-knockdown cells ($n = 64$). (C) $[Ca^{2+}]_{cyt}$ responses to Ca^{2+} readdition after Ca^{2+} store depletion in control (thin line) and WFS1-overexpressing (thick line) cells. Traces are averages of 51 control and 65 WFS1-overexpressing cells from three experiments. (D) AUCs in response to Ca^{2+} readdition in (C) were quantified. Gray bar, control cells ($n = 51$); Black bar, WFS1-overexpressing cells ($n = 65$). (E) Carbachol-stimulated $[Ca^{2+}]_{cyt}$ increases in control (thin line: $n = 39$) and WFS1-overexpressing (thick line: $n = 40$) cells. (F) Ca^{2+} influx was evaluated by Mn^{2+} quench assay in WFS1-knockdown cells. Traces are averages of 96 control (thin line) and 109 knockdown (thick line) cells from six experiments. (G) $[Ca^{2+}]_{mt}$ responses to Ca^{2+} readdition after ER store depletion in control (thin line) and WFS1-knockdown (thick line) cells. Traces are representative of 7 perfusions. (H) $[Ca^{2+}]_{mt}$ responses to Ca^{2+} readdition after ER store depletion in control (thin line) and WFS1-overexpressing (thick line) cells. Traces are representative of seven perfusions. $^{***}P < 0.001$.

for activating SOC influx [19]. However, reduced ER Ca^{2+} levels were not always associated with a decrease in SOC entry; reduced ER Ca^{2+} levels without alteration in SOC entry were reported in BAX and BAK double-knockout cells [22]. In addition to changes in cytosolic Ca^{2+} dynamics, increased Ca^{2+} uptake into mitochondria was observed upon Ca^{2+} readdition after CPA-induced store depletion in WFS1-overexpressing cells. A simple explanation for this was that the increased Ca^{2+} uptake might be due to elevated SOC influx. Alternatively, increased $[Ca^{2+}]_{er}$ might enhance Ca^{2+} supply to the mitochondria upon store depletion and activated mitochondrial function. The close relationship between the ER and mitochondria was recently established [23], and supports this notion. Further studies are needed to clarify the relation between the ER Ca^{2+} store filling state and responses of $[Ca^{2+}]_{cyt}$ and $[Ca^{2+}]_{mt}$ in WFS1-knockdown and -overexpressing cells.

The present data indicate WFS1 protein, an enigmatic protein, to play a role in regulating cellular Ca^{2+} homeostasis, at least partly, by modifying the filling state of the ER Ca^{2+} store. Our previous results demonstrated that WFS1-deficiency causes increased ER-stress in pancreatic β-cells but not in cells from the heart, skeletal muscle or brown adipose tissues [13]. In pancreatic β-cells, which produce large quantities of insulin, there is a greater load on the ER. Impaired ER Ca^{2+} homeostasis is known to cause or exacerbate ER stress [24]. It is possible that combined effects of reduced $[Ca^{2+}]_{er}$ and a greater load on the ER induce ER stress specifically in β-cells. Our present data, thus, provide clues to elucidating not only WFS1 functions but also the molecular mechanisms underlying β-cell failure in Wolfram syndrome.

Acknowledgements: We thank Prof. T. Pozzan (University of Padua) for generously providing ER-targeted aequorin cDNA, Prof. H. Takeshima (Kyoto University) for advice on the Ca^{2+} measurements, and Dr. Kanzaki for help with confocal microscopy experiments. We are also grateful to Y. Nagura and K. Tanaka for their expert assistance. This work was supported by Grants-in-Aid for Scientific Research (17590264 to H.I. and 17390258 to Y.O.) from the Ministry of Education, Science, Sports and Culture of Japan.

References

[1] Berridge, M.J., Lipp, P. and Bootman, M.D. (2000) The versatility and universality of calcium signalling. Nat. Rev. Mol. Cell Biol. 1, 11–21.
[2] Rizzuto, R. and Pozzan, T. (2003) When calcium goes wrong: genetic alterations of a ubiquitous signaling route. Nat. Genet. 34, 135–141.
[3] Meldolesi, J. and Pozzan, T. (1998) The endoplasmic reticulum Ca^{2+} store: a view from the lumen. Trends Biochem. Sci. 23, 10–14.
[4] Parekh, A.B. and Putney Jr., J.W. (2005) Store-operated calcium channels. Physiol. Rev. 85, 757–810.
[5] Schroder, M. and Kaufman, R.J. (2005) The mammalian unfolded protein response. Annu. Rev. Biochem. 74, 739–789.
[6] Wolfram, D.J. and Wagener, H.P. (1938) Diabetes mellitus and simple optic atrophy among siblings: report on four cases. Mayo. Clinic Proc. 13, 715–718.
[7] Inoue, H., Tanizawa, Y., Wasson, J., Behn, P., Kalidas, K., Bernal-Mizrachi, E., Mueckler, M., Marshall, H., Donis-Keller, H., Crock, P., Rogers, D., Mikuni, M., Kumashiro, H., Higashi, K., Sobue, G., Oka, Y. and Permutt, M.A. (1998) A gene encoding a transmembrane protein is mutated in patients with diabetes mellitus and optic atrophy (Wolfram syndrome). Nat. Genet. 20, 143–148.
[8] Strom, T.M., Hortnagel, K., Hofmann, S., Gekeler, F., Scharfe, C., Rabl, W., Gerbitz, K.D. and Meitinger, T. (1998) Diabetes insipidus, diabetes mellitus, optic atrophy and deafness (DIDMOAD) caused by mutations in a novel gene (wolframin) coding for a predicted transmembrane protein. Hum. Mol. Genet. 7, 2021–2028.
[9] Hofmann, S., Philbrook, C., Gerbitz, K.D. and Bauer, M.F. (2003) Wolfram syndrome: structural and functional analyses of mutant and wild-type wolframin, the WFS1 gene product. Hum. Mol. Genet. 12, 2003–2012.
[10] Takeda, K., Inoue, H., Tanizawa, Y., Matsuzaki, Y., Oba, J., Watanabe, Y., Shinoda, K. and Oka, Y. (2001) WFS1 (Wolfram syndrome 1) gene product: predominant subcellular localization to endoplasmic reticulum in cultured cells and neuronal expression in rat brain. Hum. Mol. Genet. 10, 477–484.
[11] Ishihara, H., Takeda, S., Tamura, A., Takahashi, R., Yamaguchi, S., Takei, D., Yamada, T., Inoue, H., Soga, H., Katagiri, H., Tanizawa, Y. and Oka, Y. (2004) Disruption of the WFS1 gene in mice causes progressive beta-cell loss and impaired stimulus-secretion coupling in insulin secretion. Hum. Mol. Genet. 13, 1159–1170.
[12] Riggs, A.C., Bernal-Mizrachi, E., Ohsugi, M., Wasson, J., Fatrai, S., Welling, C., Murray, J., Schmidt, R.E., Herrera, P.L. and Permutt, M.A. (2005) Mice conditionally lacking the Wolfram gene in pancreatic islet beta cells exhibit diabetes as a result of enhanced endoplasmic reticulum stress and apoptosis. Diabetologia 48, 2313–2321.
[13] Yamada, T., Ishihara, H., Tamura, A., Takahashi, R., Yamaguchi, S., Takei, D., Tokita, A., Satake, C., Tashiro, F., Katagiri, H., Aburatani, H., Miyazaki, J. and Oka, Y. (2006) WFS1-deficiency increases endoplasmic reticulum stress, impairs cell cycle progression and triggers the apoptotic pathway specifically in pancreatic β-cells. Hum. Mol. Genet. 15, 1600–1609.
[14] Osman, A.A., Saito, M., Makepeace, C., Permutt, M.A., Schlesinger, P. and Mueckler, M. (2003) Wolframin expression induces novel ion channel activity in endoplasmic reticulum membranes and increases intracellular calcium. J. Biol. Chem. 278, 52755–52762.
[15] Montero, M., Brini, M., Marsault, R., Alvarez, J., Sitia, R., Pozzan, T. and Rizzuto, R. (1995) Monitoring dynamic changes in free Ca^{2+} concentration in the endoplasmic reticulum of intact cells. EMBO J. 14, 5467–5475.
[16] Rizzuto, R., Simpson, A.W., Brini, M. and Pozzan, T. (1992) Rapid changes of mitochondrial Ca^{2+} revealed by specifically targeted recombinant aequorin. Nature 358, 325–327.
[17] Grynkiewicz, G., Poenie, M. and Tsien, R.Y. (1985) A new generation of Ca^{2+} indicators with greatly improved fluorescence properties. J. Biol. Chem. 260, 3440–3450.
[18] Kass, G.E., Llopis, J., Chow, S.C., Duddy, S.K. and Orrenius, S. (1990) Receptor-operated calcium influx in rat hepatocytes: identification and characterization using manganese. J. Biol. Chem. 265, 17486–17492.
[19] Pinton, P., Ferrari, D., Magalhaes, P., Schulze-Osthoff, K., Di Virgilio, F., Pozzan, T. and Rizzuto, R. (2000) Reduced loading of intracellular Ca^{2+} stores and downregulation of capacitative Ca^{2+} influx in Bcl-2-overexpressing cells. J. Cell Biol. 148, 857–862.
[20] Foyouzi-Youssefi, R., Arnaudeau, S., Borner, C., Kelley, W.L., Tschopp, J., Lew, D.P., Demaurex, N. and Krause, K.H. (2000) Bcl-2 decreases the free Ca^{2+} concentration within the endoplasmic reticulum. Proc. Natl. Acad. Sci. USA 97, 5723–5728.
[21] Zatti, G., Burgo, A., Giacomello, M., Barbiero, L., Ghidoni, R., Sinigaglia, G., Florean, C., Bagnoli, S., Binetti, G., Sorbi, S., Pizzo, P. and Fasolato, C. (2006) Presenilin mutations linked to familial Alzheimer's disease reduce endoplasmic reticulum and Golgi apparatus calcium levels. Cell Calcium 39, 539–550.
[22] Scorrano, L., Oakes, S.A., Opferman, J.T., Cheng, E.H., Sorcinelli, M.D., Pozzan, T. and Korsmeyer, S.J. (2003) BAX and BAK regulation of endoplasmic reticulum Ca^{2+}: a control point for apoptosis. Science 300, 135–139.
[23] Rizzuto, R., Duchen, M.R. and Pozzan, T. (2004) Flirting in little space: the ER/mitochondria Ca^{2+} liaison. Sci. STKE 215, 1–9.
[24] Verkhratsky, A. and Toescu, E.C. (2003) Endoplasmic reticulum Ca^{2+} homeostasis and neuronal death. J. Cell. Mol. Med. 7, 351–361.

Diabetologia (2006) 49:2217–2218
DOI 10.1007/s00125-006-0313-5

RESEARCH LETTER

Plasma concentrations of vascular endothelial growth factor are associated with peripheral oedema in patients treated with thiazolidinedione

M. Emoto · N. Fukuda · Y. Nakamori · A. Taguchi · S. Okuya · Y. Oka · Y. Tanizawa

Received: 20 April 2006 / Accepted: 24 April 2006 / Published online: 1 July 2006

To the Editor Thiazolidinediones are widely used in patients with type 2 diabetes. In addition to lowering plasma glucose, this class of drugs may reduce the risk of cardiovascular diseases in patients with diabetes. Despite the beneficial effect of thiazolidinediones, their use is sometimes associated with peripheral oedema. This is the most frequent adverse effect leading to discontinued treatment with thiazolidinediones in Japan. However, the mechanism by which thiazolidinediones induce oedema remains to be established.

Recently, Guan et al. reported that, in a mouse model, thiazolidinediones caused fluid retention through peroxisome proliferator-activated receptor-γ stimulation of renal salt absorption mediated by epithelial Na^+ channel (ENaC) [1]. The authors speculated that an increase in plasma volume causes thiazolidinedione-induced peripheral oedema. We, however, doubt that this is the sole cause of oedema in humans. ENaC is a sodium channel located in collecting tubules. This channel is also the site of action of the hormone aldosterone, a mineralocorticoid that increases sodium reabsorption. Primary aldosteronism is a disease caused by hypersecretion of this hormone. Due to excess sodium reabsorption, the circulating blood volume increases. The resulting headache and hypertension are well documented. However, peripheral oedema does not usually develop [2]. This is a well-known outcome of this disease. Oedema, moreover, also does not develop as a result of the increased plasma volume in the syndrome of inappropriate secretion of antidiuretic hormone [3]. Antidiuretic horomone is a pituitary hormone that activates the water channel aquaporin 2 in collecting tubules, thereby increasing water reabsorption. These observations in relation to endocrine diseases suggest that blood volume expansion is not sufficient for peripheral oedema to develop.

We would like to highlight another important factor that might also be involved in the process. Previously, we reported that thiazolidinediones increase the plasma levels of vascular endothelial growth factor (VEGF) [4]. Since VEGF is a potent vascular permeability factor, an increase in VEGF levels may contribute to thiazolidinedione-induced oedema. However, because of the difficulty of quantifying the severity of oedema, no one has demonstrated a clear correlation between peripheral oedema and plasma VEGF levels. Assessing the presence of peripheral oedema by body weight can be misleading, because thiazolidinediones increase body fat mass [5] and circulating blood volume [1]. In our previous report, for example, a weak correlation between body weight and plasma VEGF concentration was observed only in female patients, but not in male patients or groups comprising both sexes [4].

Here, we demonstrate a strong correlation between clinically apparent peripheral oedema and plasma VEGF concentration. Oedema is defined as a clinically apparent increase in the interstitial fluid volume. Thus, we judged the existence of peripheral oedema by the presence of pitting after pressure was applied to the bilateral lower extremities. We re-evaluated the clinical data collected for our previous study [4]. Briefly, a total of 30 patients with type 2 diabetes

M. Emoto · N. Fukuda · Y. Nakamori · A. Taguchi · S. Okuya · Y. Tanizawa (✉)
Division of Endocrinology, Metabolism, Hematological Sciences and Therapeutics, Department of Bio-Signal Analysis, Yamaguchi University Graduate School of Medicine, 1-1-1, Minami-Kogushi, Ube 755-8505, Japan
e-mail: tanizawa@yamaguchi-u.ac.jp

Y. Oka
Division of Molecular Metabolism and Diabetes, Tohoku University Graduate School of Medicine, Sendai, Japan

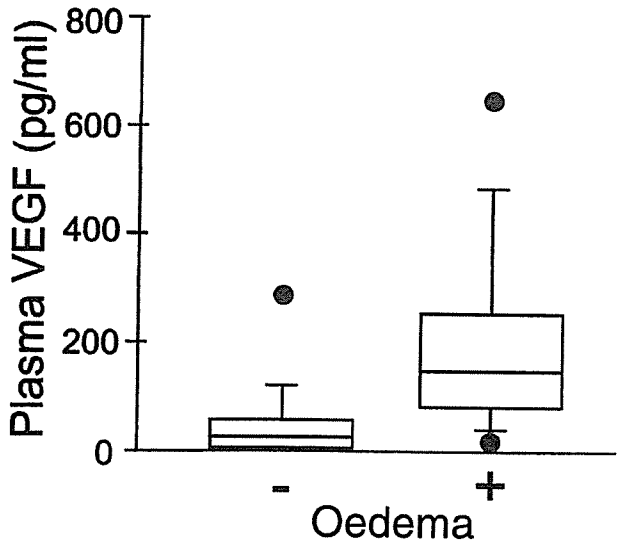

Fig. 1 Plasma vascular endothelial growth factor (*VEGF*) increase in patients with peripheral oedema. Plasma VEGF concentrations were measured in patients with and without peripheral oedema, as determined by physical examination. Concentrations were elevated in patients with (+) peripheral oedema. Data are medians, 70th and 90th percentiles. p=0.0011, n=12 in each group, Mann–Whitney test

(12 men and 18 women, mean age 55.9± 13.9 years), who had already been treated with troglitazone (the first thiazolidinedione compound) 400 mg daily for 3–6 months, participated in the study. No one had a history of congestive heart failure or was receiving combination therapy with insulin. Patients with cancer, liver cirrhosis, nephrotic syndrome or varicose veins were excluded. We measured total circulating $VEGF_{165/121}$ isoforms in platelet-poor EDTA-plasma. Based on clinical records, the patients treated with troglitazone were divided into two groups in a binary manner. One comprised patients who had peripheral oedema determined by physical examination; the other patients who did not. In some patients, we were uncertain whether they had oedema or not. These patients were excluded from the study (plasma VEGF 66.1 pg/ml [median]; n=6). As shown in Fig. 1, the plasma $VEGF_{165/121}$ concentration was significantly higher in patients with than in those without oedema (with 164.5 pg/ml, without 33.2 pg/ml [median], respectively; p=0.0011; n=12 in each group). None of the patients had peripheral oedema at the outset, either in the troglitazone group, or in the control groups (patients treated by diet alone, sulfonylurea, and insulin; n=10 in each group). Moreover, reversal of oedema and plasma VEGF concentration was observed after discontinuation of treatement with troglitazone. Our present data suggest that increased plasma VEGF is one of the major factors of thiazolidinedione-induced peripheral oedema.

On the other hand, it is also true that the patients treated with thiazolidinediones had mild haemodilution [6]. This clinical observation suggests that other fluid dynamic factors may be involved in the development of oedema. VEGF disrupts vascular barrier function, and endothelial cells exposed to VEGF allow passage of particles of different sizes by a variety of mechanisms. In this pathological condition, vascular leakage is thought to be dependent on relative pressure gradients between the vascular and extra-vascular compartments [7]. If renal salt absorption is increased and microvascular pressure is high relative to interstitial pressure, capillary leakage may be clinically evident. These pathophysiological consequences are consistent with the idea that both VEGF-enhanced vascular permeability and ENaC-mediated fluid retention are necessary for thiazolidinediones to induce peripheral oedema. Other thiazolidinediones such as pioglitazone also increase plasma VEGF concentrations [8, unpublished observation by the authors]. However, Tooke et al. argued against this point in a recent online publication [9]. In any case, since oedema is one of the major factors for discontinuing treatment with thiazolidinediones, further studies are needed to develop safer and better tolerated new thiazolidinediones.

In summary, we hypothesised that the mechanism of thiazolidinedione-induced peripheral oedema involves the synergistic effect of water retention and hyperpermeability.

References

1. Guan Y, Hao C, Cha DR et al (2005) Thiazolidinediones expand body fluid volume through PPARγ stimulation of ENaC-mediated renal salt absorption. Nat Med 11:861–866
2. Williams GH, Dluhy RG (2005) Disorders of the adrenal cortex. In: Kasper DL et al. (eds) Harrison's principles of internal medicine, 16th edn. McGraw-Hill, New York, pp 2138–2140
3. Bartter FC, Schwartz WB (1967) The syndrome of inappropriate secretion of antidiuretic hormone. Am J Med 42:790–806
4. Emoto M, Anno T, Sato Y et al (2001) Troglitazone treatment increases plasma vascular endothelial growth factor in diabetic patients and its mRNA in 3T3-L1 adipocytes. Diabetes 50:1166–1170
5. Kelly IE, Han TS, Walsh K, Lean ME (1999) Effects of a thiazolidinedione compound on body fat and fat distribution of patients with type 2 diabetes. Diabetes Care 22:288–293
6. Hollenberg NK (2003) Considerations for management of fluid dynamic issues associated with thiazolidinediones. Am J Med 115 (Suppl 8A):111S–115S
7. Weis SM, Cheresh DA (2005) Pathophysiological consequences of VEGF-induced vascular permeability. Nature 437:497–504
8. Baba T, Shimada K, Neugebauer S et al (2001) The oral insulin sensitizer, thiazolidinedione, increases plasma vascular endothelial growth factor in type 2 diabetic patients. Diabetes Care 24:953–954
9. Tooke JE, Elston LM, Gooding KM et al (2006) The insulin sensitiser pioglitazone does not influence skin microcirculatory function in patients with type 2 diabetes treated with insulin. Diabetologia 49:1064–1070

0013-7227/06/$15.00/0
Printed in U.S.A.

Endocrinology 147(12):5893–5900

doi: 10.1210/en.2006-0418

Hyperphagia Alters Expression of Hypothalamic 5-HT2C and 5-HT1B Receptor Genes and Plasma Des-Acyl Ghrelin Levels in A^y Mice

Katsunori Nonogaki, Kana Nozue, and Yoshitomo Oka

Center of Excellence, Division of Molecular Metabolism and Diabetes, Tohoku University Graduate School of Medicine, Miyagi 980-8575, Japan

The central melanocortin (MC) pathway is suggested to mediate satiety signaling downstream of serotonin (5-HT)2C receptors. 5-HT2C receptor mutant mice consume more food, which leads to late-onset obesity and impaired glucose tolerance. A^y mice with ectopic expression of the agouti peptide, which leads to a perturbation of the central MC pathway, develop obesity and diabetes, associated with low levels of plasma total ghrelin. Here, we report that 5-wk-old A^y mice consumed more food in association with decreases in levels of plasma des-acyl ghrelin, but not active ghrelin, and increases in hypothalamic 5-HT2C and 5-HT1B receptor gene expression compared with wild-type mice matched for age and body weight. These alterations were also observed in 8-wk-old obese A^y mice. Restricted feeding significantly decreased hypothalamic 5-HT2C and 5-HT1B receptor gene expression in association with a reversal of the decreases in plasma des-acyl ghrelin levels in 5-wk-old A^y mice. Moreover, restricted feeding reduced body weight, hyperinsulinemia, and hyperglycemia in association with increases in plasma des-acyl ghrelin levels in 8-wk-old obese A^y mice. Administration of *m*-chlorophenylpiperazine and fenfluramine, both of which induce anorexic effects via 5-HT2C receptors and/or 5-HT1B receptors, suppressed food intake in 5- and 8-wk-old A^y mice, whereas the anorexic effects were attenuated in food-restricted A^y mice. These findings suggest that the agouti peptide down-regulates hypothalamic 5-HT2C and 5-HT1B receptor gene expression under restricted feeding conditions, whereas chronic hyperphagia increases the expression of these genes and decreases plasma des-acyl ghrelin levels in A^y mice. (*Endocrinology* 147: 5893–5900, 2006)

HYPERPHAGIA IS A risk factor for obesity and type 2 diabetes mellitus, both of which are increasing at alarming rates in industrialized countries, including Japan and the United States. Management of eating behavior is an important therapeutic strategy for obesity and type 2 diabetes.

Brain serotonin (5-hydroxytryptamine; 5-HT), systems contribute to regulate eating behavior and energy homeostasis (1–4). 5-HT2C receptors and/or 5-HT1B receptors contribute to mediate the appetite-suppressing effects of 5-HT drugs, such as *m*-chlorophenylpiperazine (mCPP) and *d*-fenfluramine (2, 5–7). 5-HT2C receptor mutant mice display leptin-independent hyperphagia that leads to late-onset obesity and impaired glucose tolerance (3).

The central melanocortin (MC) pathway is suggested to mediate satiety signaling downstream of 5-HT2C receptors (8). A^y mice have dominant alleles at the agouti locus (*A*), which produces ectopic expression of the agouti peptide, an antagonist of the hypothalamic MC4 receptors and MC3 receptors (9–11), and display hyperphagia and obesity. A^y mice are reportedly resistant to the anorexic effects induced by leptin and fenfluramine (8, 12, 13). In addition, obese A^y mice have lower levels of plasma ghrelin, an orexigenic peptide secreted from the stomach, than wild-type mice (14).

Ghrelin stimulates GH secretion and food intake (15). Fasting increases plasma ghrelin levels, whereas feeding reduces plasma ghrelin levels in normal animals and humans (15). Plasma ghrelin levels are also higher in patients with anorexia nervosa and lower in obese subjects than in normal individuals (15). It is therefore reasonable that plasma total ghrelin levels are lower in obese A^y mice (14). Ghrelin has two forms, however: active *n*-octanoyl-modified ghrelin and nonactive des-acyl ghrelin. Plasma active and des-acyl ghrelin levels during the development of obesity in A^y mice have not been evaluated.

To determine the effects of the agouti peptide on plasma active and des-acyl ghrelin levels and 5-HT signaling of satiety, we examined plasma levels of active ghrelin and des-acyl ghrelin and hypothalamic 5-HT2C and 5-HT1B receptor gene expression in food-unrestricted and food-restricted A^y mice and wild-type mice matched for age. In addition, to determine the role of hyperphagia in obesity and diabetes in A^y mice, we examined the effects of restricted feeding on obesity and diabetes in A^y mice. Moreover, to determine whether A^y mice are sensitive to 5-HT2C and/or 5-HT1B receptor stimulation-induced feeding suppression, we examined the effects of mCPP, a 5-HT2C receptor agonist, and fenfluramine, a 5-HT reuptake inhibitor and releaser that induces anorexic effects via 5-HT2C receptors and/or 5-HT1B receptors, on food intake in A^y mice.

First Published Online September 14, 2006

Abbreviations: AGRP, Agouti-related peptide; CART, cocaine- and amphetamine-regulated transcript; 5-HT, serotonin (5-hydroxytryptamine); MC, melanocortin; mCPP, *m*-chlorophenylpiperazine; NPY, neuropeptide Y; POMC, proopiomelanocortin.

***Endocrinology* is published monthly by The Endocrine Society (http://www.endo-society.org), the foremost professional society serving the endocrine community.**

Materials and Methods

General procedures

Animals were purchased from Japan CLEA (Tokyo, Japan). Mice were housed in individual cages with free access to water and chow

pellets in a light-controlled (12 h on/12 h off; lights off at 2000 h) and temperature-controlled (20–22 C) environment.

In the first experiment, age- and body-weight-matched male 5-wk-old wild-type mice (25.9 ± 0.4 g) and A^y mice (25.8 ± 0.4 g),and age-matched 8-wk-old wild-type mice (31.5 ± 0.5 g) and A^y mice (37.9 ± 0.9 g) were used. Daily food intake of the mice was measured. Animals were decapitated and blood was collected between 1000 and 1100 h. The hypothalamus, cerebral cortex, and medulla oblongata were removed to determine mRNA levels, and plasma active ghrelin and des-acyl ghrelin levels were measured. Plasma was immediately frozen and stored at −80 C until assayed for active and des-acyl ghrelin. Plasma des-acyl ghrelin levels were also measured after a 24-h fast in 5-wk-old wild-type mice (23.3 ± 0.3 g) and in 5-wk-old A^y mice (22.4 ± 0.3 g).

In the second experiment, plasma active ghrelin and des-acyl ghrelin levels and hypothalamic 5-HT2C and 5-HT1B receptor gene expression were measured in 5-wk-old A^y mice (19.7 ± 0.2 g) and wild-type mice (19.8 ± 0.4 g), which were provided 3.5 g chow pellets daily for 5 d before the experiment. Animals were decapitated, and blood was collected between 1000 and 1100 h. Plasma was immediately frozen and stored at −80 C until assayed for active and des-acyl ghrelin.

In the third experiment, 5-wk-old male A^y mice and wild-type littermates, which were provided 3.5 g chow pellets daily for 5 d before the experiment, were ip injected with saline or mCPP (5 mg/kg). Chow pellets were provided 30 min later. Intake of chow pellets was measured for the next hour. The experiment was performed between 1000 and 1200 h.

In the fourth experiment, body weight, blood glucose, plasma active ghrelin, and des-acyl ghrelin levels were measured in 8-wk-old A^y mice, which were provided 3.5 g chow pellets daily for 3 d, and freely fed A^y mice. Animals were decapitated, and blood was collected between 1000 and 1100 h. Blood glucose was measured using a glucose strip (Freestyle, Kissei, Japan). Plasma was immediately frozen and stored at −80 C until assayed for insulin and active and des-acyl ghrelin.

In the fifth experiment, 5-wk-old male A^y mice and wild-type littermates were ip injected with saline or mCPP (5 mg/kg) or fenfluramine (3 mg/kg) 30 min before the onset of the dark cycle. The intake of chow pellets was measured for the next hour after the onset of the dark cycle.

Finally, 8-wk-old male A^y mice and wild-type littermates were ip injected with saline or mCPP (5 mg/kg) twice daily (at 1000 and 1800 h) for 3 d. Daily food intake and body weight were measured.

The doses of mCPP (5 mg/kg) and fenfluramine (3 mg/kg) were selected based on the evidence that mCPP or fenfluramine-induced hypophagia was attenuated by a genetic blockade of 5-HT2C receptors (2, 5).

Plasma ghrelin and insulin assays

Plasma active ghrelin levels were measured by ELISA (active ghrelin ELISA kit and des-acyl ghrelin ELISA kit; Mitsubishi Kagaku Iatron Inc., Tokyo, Japan). For the ELISA of active ghrelin, 1 N hydrogen chloride was added to the samples at a final concentration of 0.1 N immediately after plasma separation. Plasma insulin levels were measured using a rat insulin RIA kit (Linco, St. Louis, MO).

The animal studies were conducted under protocols in accordance with the institutional guidelines for animal experiments at Tohoku University Graduate School of Medicine.

Real-time quantitative RT-PCR

Total RNA was isolated from mouse hypothalamic tissue using the RNeasy Midi kit (QIAGEN, Hilden, Germany) according to the manufacturer's directions, and cDNA synthesis was performed using the SuperScript III First-Strand Synthesis System for RT-PCR Kit (Invitrogen, Rockville, MD) using 1 μg total RNA. cDNA synthesized from total RNA was evaluated in a real-time PCR quantitative system (LightCycler Quick System 350S; Roche Diagnostics, Mannheim, Germany). The primers used were as follows: mouse proopiomelanocortin (POMC), sense, 5′-ATA GAT GTG TGG AGC TGG TG-3′, and antisense, 5′-GGC TGT TCA TCT CCG TTG-3′; for mouse cocaine- and amphetamine-regulated transcript (CART), sense, 5′-CTG GAC ATC TAC TCT GCC GTG G-3′, and antisense, 5′-GTT CCT CGG GGA CAG TCA CAC AGC-3; for mouse neuropeptide Y (NPY), sense, 5′-GCT TGA AGA CCC TTC CAT TGG TG-3′, and antisense, 5′-GGC GGA GTC CAG CCT AGT GG-3′; for mouse agouti-related peptide (AGRP), sense, 5′-CAG ACC GAG CAG AAG AAG-3′, and antisense, 5′-GAC TCG TGC AGC CTT ACA-3′; for mouse orexin, sense, 5′-CTC CTT CAG GCC AAC GGT A-3′, and antisense, 5′-GTG GTA GTT ACG GTC GGA CA-3′; for mouse 5-HT1B receptor, sense, 5′-TGC CTG CTG GTT TCA CAT-3′, 5′-ATA GAT GTG TGG AGC TGG TG-3′, and antisense, 5′-GCG CAC TTA AAG CGT ATC A-3′; 5-HT2C receptor, sense, 5′-CTG AGG GAC GAA AGC AAA G-3′, and antisense, 5′-CAC ATA GCC AAT CCA AAC AAA C-3′; and for mouse β-actin, sense, 5′-TTG TAA CCA ACT GGG ACG ATA TGG-3′, and antisense, 5′-GAT CTT GAT CTT CAT GGT GCT AGG-3′. The relative amount of mRNA was calculated using β-actin mRNA as the invariant control. The data are shown as the fold change of the mean value of the control group, which received saline.

Data are presented as the mean values ± SEM (n = 5–8). Comparisons between two groups were performed using two-tailed unpaired Student's *t* test. A *P* value of less than 0.05 was considered statistically significant.

Results

Plasma active and des-acyl ghrelin levels in A^y mice

To exclude the effects of differences in body weight, we evaluated plasma active and des-acyl ghrelin levels in 5-wk-old A^y mice and wild-type mice matched for age and body weight. There were no genotypic differences in plasma active ghrelin levels, whereas plasma des-acyl ghrelin levels in A^y mice were lower than those in wild-type mice (Fig. 1, A and B). Five-week-old A^y mice consumed more food than wild-type mice (Fig. 1C). In addition, plasma des-acyl ghrelin levels in A^y mice were lower than those in wild-type mice after a 24-h fast (Fig. 1D).

There were decreased plasma des-acyl ghrelin levels in 8-wk-old obese A^y mice compared with wild-type mice (Fig. 2B), whereas there were no genotypic differences in plasma active ghrelin levels between 8-wk-old obese A^y mice and wild-type mice (Fig. 2A). Eight-week-old A^y mice consumed more food and had significantly higher body weight compared with age-matched wild-type mice (Fig. 2, C and D).

Alterations of hypothalamic neuropeptide mRNA levels in A^y mice

To determine the relationship between plasma des-acyl ghrelin levels and the expression of hypothalamic neuropeptide genes involved in regulating feeding and energy homeostasis, we examined the gene expression of hypothalamic NPY, AGRP, orexin (orexigenic peptides), POMC, and CART (anorexigenic peptides), which are major neuropeptides involved in the regulation of feeding behavior (16). There were no significant differences in hypothalamic NPY and POMC mRNA levels between 5-wk-old A^y mice and wild-type mice matched for body weight, whereas hypothalamic CART, AGRP, and orexin mRNA levels were significantly decreased (0.66-, 0.73-, and 0.76-fold, respectively) (Table 1). There were no significant differences in the gene expression of these peptides between 8-wk-old A^y mice and wild-type mice (Table 1).

Alterations of hypothalamic 5-HT2C and 5-HT1B receptor mRNA levels in A^y mice

To determine the effects of agouti peptide on hypothalamic 5-HT2C and 5-HT1B receptor gene expression, we

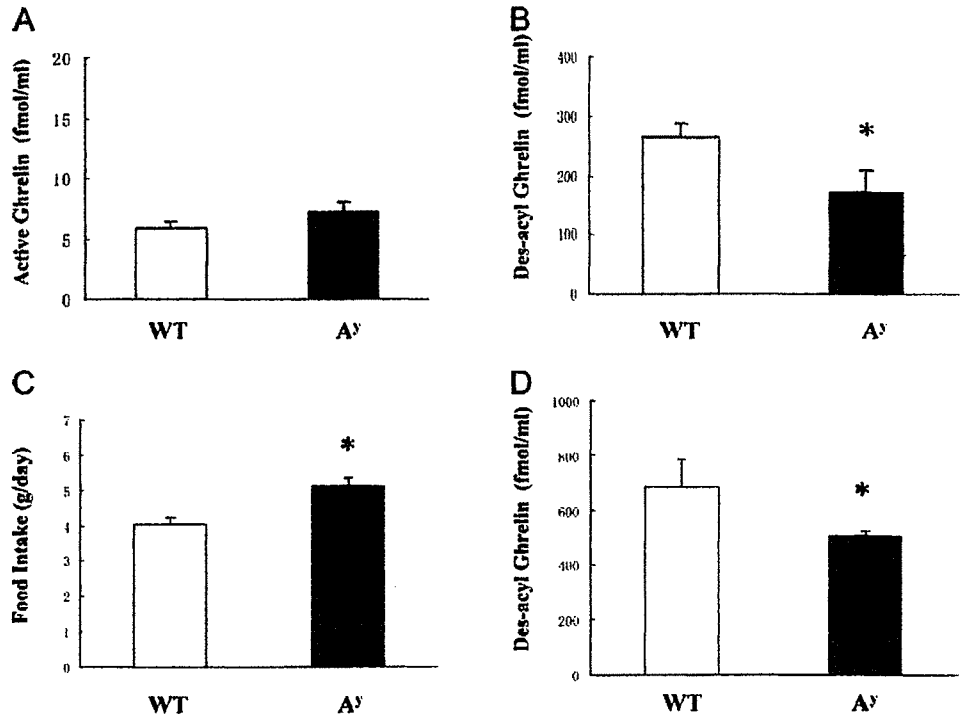

FIG. 1. Plasma active ghrelin (A) and des-acyl ghrelin levels (B) and daily food intake (C) in male 5-wk-old wild-type (WT) mice and A^y mice matched for body weight (wild-type mice, 25.9 ± 0.4 g; A^y mice, 25.8 ± 0.4 g) as described in *Materials and Methods*. Plasma des-acyl ghrelin levels were measured after a 24-h fast in 5-wk-old wild-type mice (23.3 ± 0.3 g) and in 5-wk-old A^y mice (22.4 ± 0.3 g) (D). Data are presented as the mean values ± SEM (n = 7–8). *, $P < 0.05$.

examined the expression of hypothalamic 5-HT2C and 5-HT1B receptor genes in 5- and 8-wk-old A^y mice and wild-type mice. Hypothalamic 5-HT2C and 5-HT1B receptor mRNA levels were significantly increased in 5-wk-old nonobese A^y mice compared with wild-type mice (5-HT2C receptor mRNA, 1.5-fold; 5-HT1B receptor mRNA, 2-fold) (Fig. 3A). The increases in hypothalamic 5-HT2C and 5-HT1B receptor mRNA levels were also observed in 8-wk-old obese A^y mice (5-HT2C receptor mRNA, 1.4-fold; 5-HT1B receptor mRNA, 1.4-fold; Fig. 3B). Next, we examined 5-HT2C and 5-HT1B receptor mRNA levels in the cerebral cortex and medulla oblongata where the agouti peptide is not translated. There were no significant differences in 5-HT2C and 5-HT1B receptor mRNA in the cerebral cortex and medulla oblongata between 5-wk-old A^y mice and wild-type mice (Fig. 3, C and D).

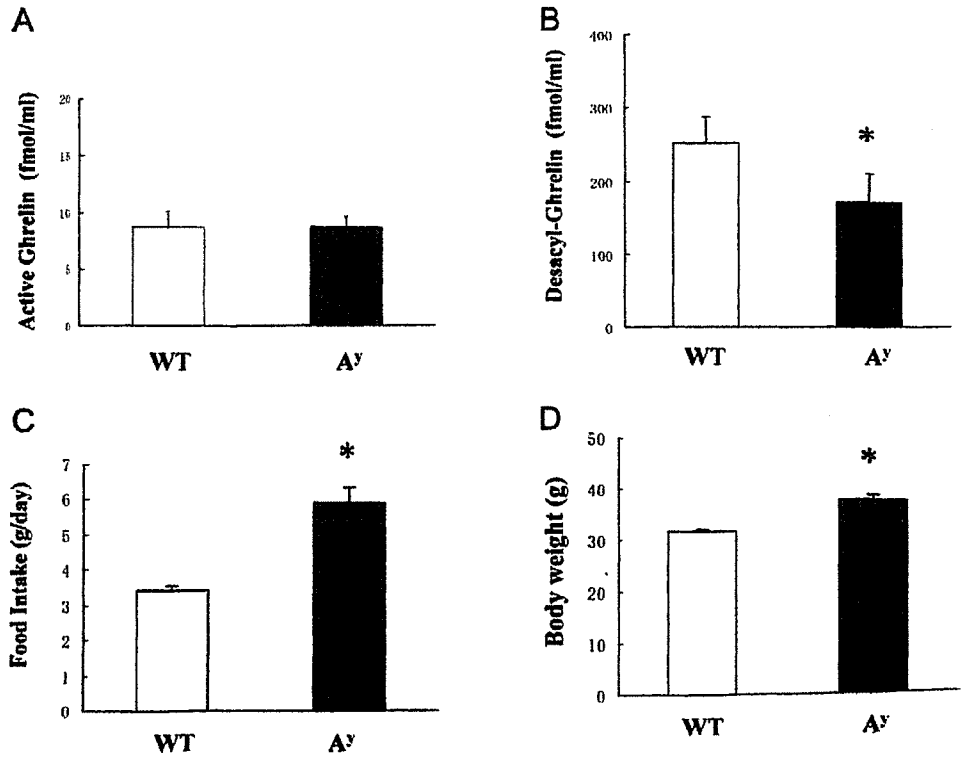

FIG. 2. Plasma active ghrelin (A) and des-acyl ghrelin levels (B), daily food intake (C), and body weight (D) in 8-wk-old A^y mice and wild-type (WT) mice as described in *Materials and Methods*. Data are presented as the mean values ± SEM (n = 7–8). *, $P < 0.05$.

TABLE 1. Hypothalamic neuropeptide mRNA levels in 5- and 8-wk-old A^y mice and wild-type mice as described in *Materials and Methods*

	5 wk old		8 wk old	
	A^y	WT	A^y	WT
POMC	1.17 ± 0.15	1.0 ± 0.16	0.98 ± 0.05	1.0 ± 0.07
CART	0.66 ± 0.04[a]	1.0 ± 0.11	1.03 ± 0.03	1.0 ± 0.07
NPY	0.95 ± 0.04	1.0 ± 0.14	1.15 ± 0.10	1.0 ± 0.07
AGRP	0.73 ± 0.05[a]	1.0 ± 0.12	0.80 ± 0.04	1.0 ± 0.10
Orexin	0.76 ± 0.09[a]	1.0 ± 0.14	1.32 ± 0.13	1.0 ± 0.06

Data are presented as the mean values ± SEM (n = 5) WT, Wild type.
[a] $P < 0.05$.

Effects of restricted feeding on plasma active and des-acyl ghrelin levels, hypothalamic 5-HT1B and 5-HT2C receptor mRNA levels, and the responsiveness to mCPP in 5-wk-old A^y mice

To determine whether the alterations of plasma des-acyl ghrelin and hypothalamic 5-HT2C and 5-HT1B receptor mRNA levels result from direct effects of the agouti peptide or to secondary effects induced by hyperphagia, we examined the effects of restricted feeding (3.5 g/d for 5 d) on plasma active and des-acyl ghrelin levels, hypothalamic 5-HT1B and 5-HT2C receptor mRNA levels, and the responsiveness to mCPP in 5 wk-old A^y mice and wild-type mice. There were no significant differences in plasma active and des-acyl ghrelin levels between the food-restricted 5 wk-old A^y mice and wild-type mice (Fig. 4, A and B). In addition, hypothalamic 5-HT2C and 5-HT1B receptor mRNA levels were significantly decreased in food-restricted A^y mice compared with wild-type mice (Fig. 4C). Both A^y mice and wild-type mice consumed 3.5 g of food during the light cycle for 5 d and were fasted during the dark cycle. After a 15-h fast, mCPP (5 mg/kg) had no effect on food intake in food-restricted A^y mice, whereas it significantly suppressed food intake in food-restricted wild-type mice (Fig. 4D).

Effects of restricted feeding on body weight, blood glucose, plasma insulin, and active and des-acyl ghrelin levels in 8-wk-old A^y mice

Restricted feeding (3.5 g/d for 3 d) significantly increased plasma des-acyl ghrelin levels in A^y mice (Fig. 5B), whereas it had no effect on plasma active ghrelin levels (Fig. 5A). In addition, restricted feeding significantly reduced body weight and normalized hyperglycemia in 8-wk-old A^y mice (Fig. 5, C and D). The blood glucose levels in food-restricted 8-wk-old A^y mice were significantly lower than those in nonobese 5-wk-old A^y (food-restricted 8-wk-old A^y mice, 127 ± 5 mg/dl; nonobese 5-wk-old A^y mice, 185 ± 8 mg/dl; n = 6 for each group; $P < 0.05$). In addition, the blood glucose levels in food-restricted 8-wk-old A^y mice were significantly lower than those in 8-wk-old wild-type mice (8-wk-old wild-type mice, 166 ± 6 mg/dl; n = 6; $P < 0.05$). Moreover, restricted feeding significantly reduced plasma insulin levels in 8-wk-old A^y mice (freely fed A^y mice, 10.8 ± 1.6 ng/ml; restricted-fed A^y mice, 2.3 ± 0.4 ng/ml; n = 6 for each group; $P < 0.05$).

Effects of mCPP and fenfluramine on food intake in A^y mice

To characterize hyperphagia in A^y mice, we examined the responsiveness to 5-HT drugs such as mCPP and fenfluramine, which cause anorexic effects via 5-HT2C receptors and/or 5-HT1B receptors, in A^y mice. Both mCPP and fenfluramine significantly suppressed food intake in A^y mice and wild-type mice (Fig. 6, A and B). In addition, chronic

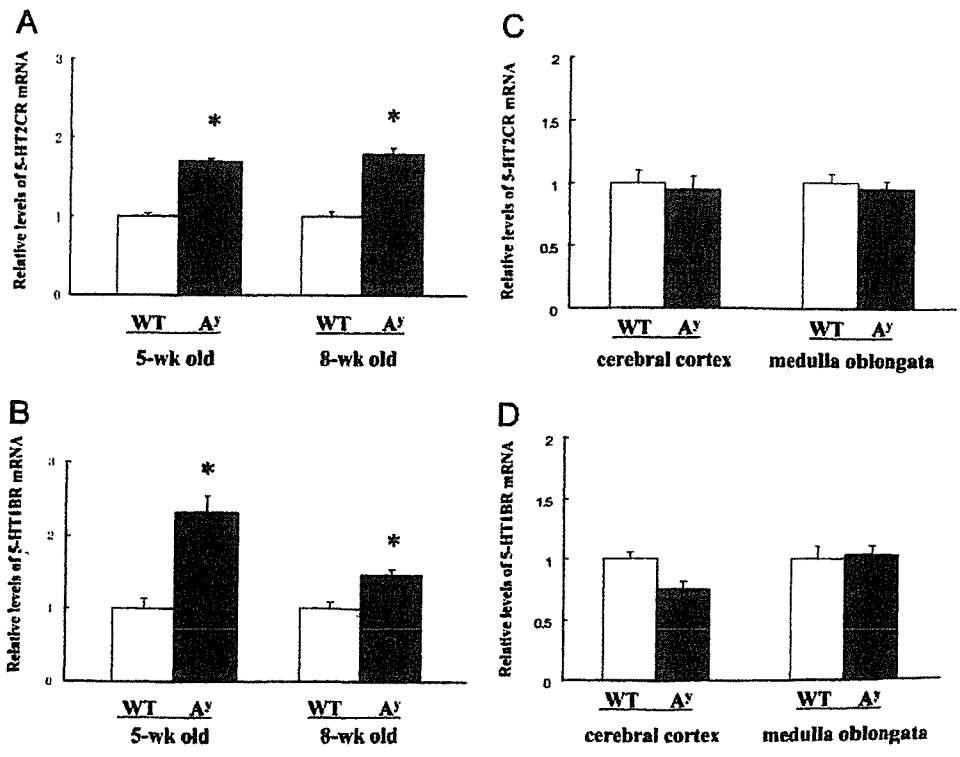

FIG. 3. 5-HT2C receptor (A) and 5-HT1B receptor (B) mRNA levels in the hypothalamus were evaluated in freely fed 5-wk-old and 8-wk-old A^y mice and wild-type (WT) mice. 5-HT2C receptor mRNA levels in cerebral cortex and medulla oblongata (C) and 5-HT1B receptor mRNA levels in cerebral cortex and medulla oblongata (D) were evaluated in freely fed 5-wk-old A^y mice and wild-type mice as described in *Materials and Methods*. Data are presented as the mean values ± SEM (n = 5). *, $P < 0.05$.

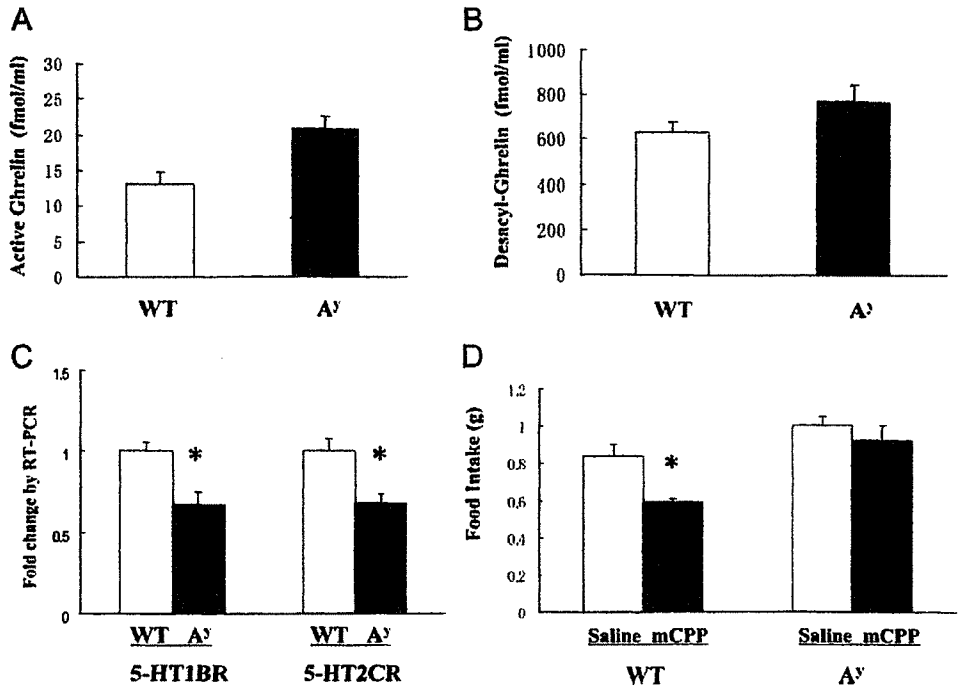

FIG. 4. Effects of restricted feeding on plasma active ghrelin (A) and des-acyl ghrelin levels (B) and hypothalamic 5-HT2C and 5-HT1B receptor mRNA levels (C) and effects of mCPP on food intake (D) in 5-wk-old A^y mice and wild-type (WT) mice. Plasma active and des-acyl ghrelin levels and hypothalamic 5-HT2C and 5-HT1B receptor mRNA levels were measured, and the drug was administered as described in *Materials and Methods*. Data are presented as the mean values ± SEM (n = 6). *, $P < 0.05$.

treatment with mCPP for 3 d decreased daily food intake (Fig. 7, A and B) and increased weight loss (Fig. 7, C and D) in both A^y mice and wild-type mice.

Discussion

The present results indicate that plasma des-acyl ghrelin levels, but not active ghrelin levels, are decreased in nonobese A^y mice that consume more food. The low plasma des-acyl ghrelin levels were observed not only in the fed state but also in a 24-h fasted state of nonobese A^y mice. Moreover, decreases in plasma des-acyl ghrelin levels were observed in 8-wk-old obese A^y mice. Thus, decreases in plasma des-acyl ghrelin, but not active ghrelin levels, preceded the development of obesity in A^y mice. In addition, restricted feeding reversed the decrease in plasma des-acyl ghrelin levels in nonobese A^y mice and increased plasma des-acyl ghrelin levels in obese A^y mice. These findings suggest that chronic hyperphagia induced by the agouti peptide, rather than the direct effects of the agouti peptide, contributed to the decreases in des-acyl ghrelin levels, leading to an increased

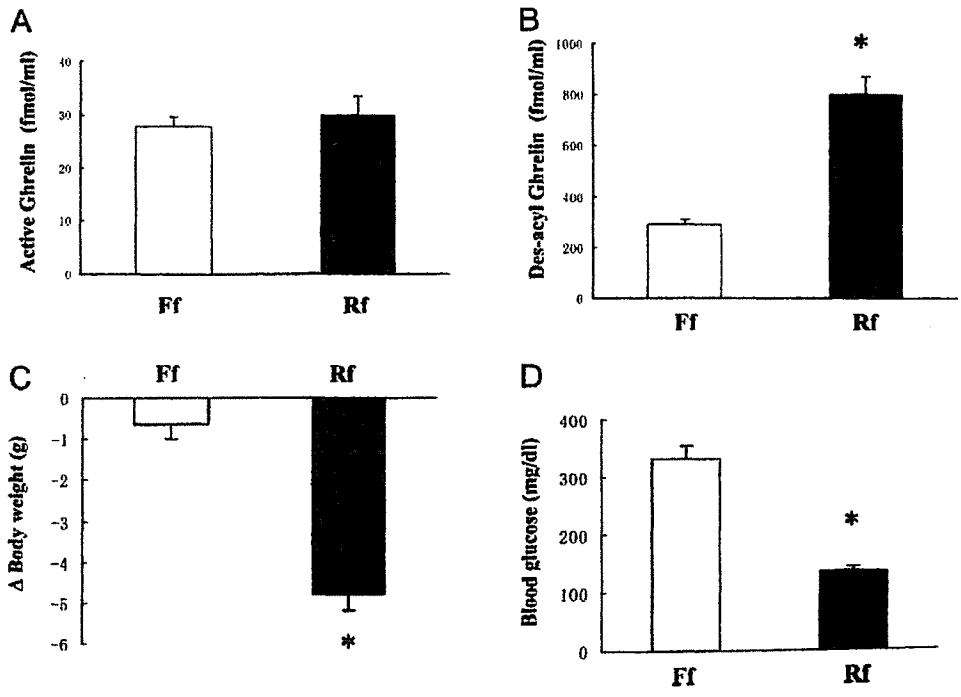

FIG. 5. Effects of restricted feeding on plasma active (A) and des-acyl ghrelin levels (B), body weight (C), and blood glucose levels (D) in 8-wk-old male A^y mice. Plasma active and des-acyl ghrelin levels and blood glucose levels were measured as described in *Materials and Methods*. Each *column* and *bar* represents the mean value ± SEM of eight mice. Ff, Freely feeding; Rf, restricted feeding. *, $P < 0.05$.

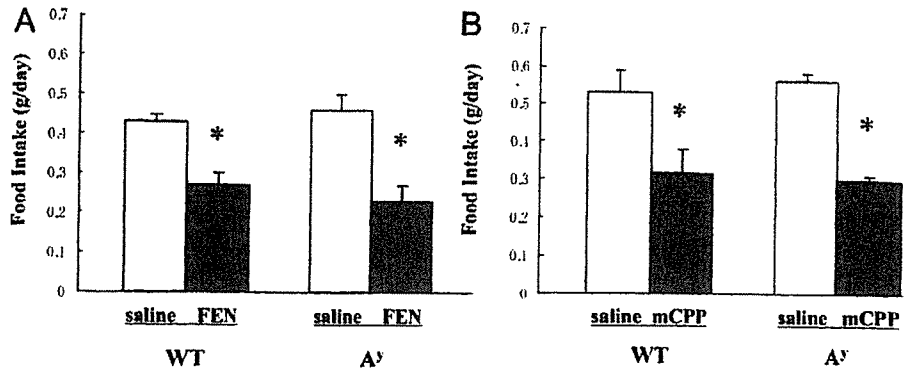

FIG. 6. Effects of mCPP (A) or fenfluramine (Fen) (B) on food intake in 5-wk-old male A^y mice and wild-type (WT) mice after onset of the dark cycle. Drugs were administered as described in *Materials and Methods*. Each *column* and *bar* represents the mean value ± SEM of seven to eight mice. *, $P < 0.05$.

ratio of active/des-acyl ghrelin. Active ghrelin is an endogenous ligand for the GH secretagogue receptor 1a, whereas des-acyl ghrelin exhibits its bioactivities via a mechanism independent of the GH secretagogue receptor 1a (15). It is therefore unlikely that des-acyl ghrelin competes with active ghrelin for binding sites.

Because the acylation of ghrelin is assumed to be essential for its actions, des-acyl ghrelin, which lacks the fatty acid modification of ghrelin, is assumed to be devoid of biological effects (15). Des-acyl ghrelin does not stimulate GH release (15). Several recent studies, however, indicate that des-acyl ghrelin has biological effects on cell proliferation, survival, and metabolism of cardiomyocytes, endothelial cells, adipocytes, myocytes, and myelocytes and on food intake (15, 17–24), although the effects of des-acyl ghrelin remain controversial. Toshinai *et al.* (20) reported that central des-acyl ghrelin increases food intake, whereas peripheral des-acyl ghrelin has no effects on food intake in rats and C57BL6J and ddy mice. Asakawa *et al.* (21) and Chen *et al.* (22) reported that either central or peripheral administration of des-acyl ghrelin suppresses food intake in ddy mice and rats.

In addition, Thompson *et al.* (23) reported that peripheral des-acyl ghrelin directly promotes adipogenesis in the bone marrow of GH-deficient dwarf (dw/dw) rats *in vivo*, whereas Zhang *et al.* (24) reported that des-acyl ghrelin inhibits adipogenesis by stimulating cell proliferation in 3T3-L1 cells. Moreover, Asakawa *et al.* (21) reported that transgenic mice overexpressing des-acyl ghrelin have reduced food intake, body weight, and fat pad mass weight accompanied by decreased linear growth, whereas Ariyasu *et al.* (25) reported that similar transgenic mice did not reduce food intake and body fat mass despite reduced longitudinal growth and body weight. Thus, the results of studies of the effects of des-acyl ghrelin on feeding and adipogenesis are not consistent. On the other hand, knockout of the ghrelin gene in mice has no effect on food intake or body weight changes during growth (26, 27). Because of the low plasma des-acyl ghrelin levels in pre-obese and obese A^y mice, it is unlikely that des-acyl ghrelin promotes food intake and adiposity in A^y mice.

In the hypothalamus, ghrelin neurons contact the cell bodies and dendrites of NPY/AGRP and POMC neurons in the arcuate nucleus (28) and orexin neurons in the lateral hypothalamus (20, 29). The present study, however, demonstrates that alterations of the expression of hypothalamic NPY, AGRP, POMC, CART, and orexin genes were not proportional to the alterations of plasma des-acyl ghrelin and the

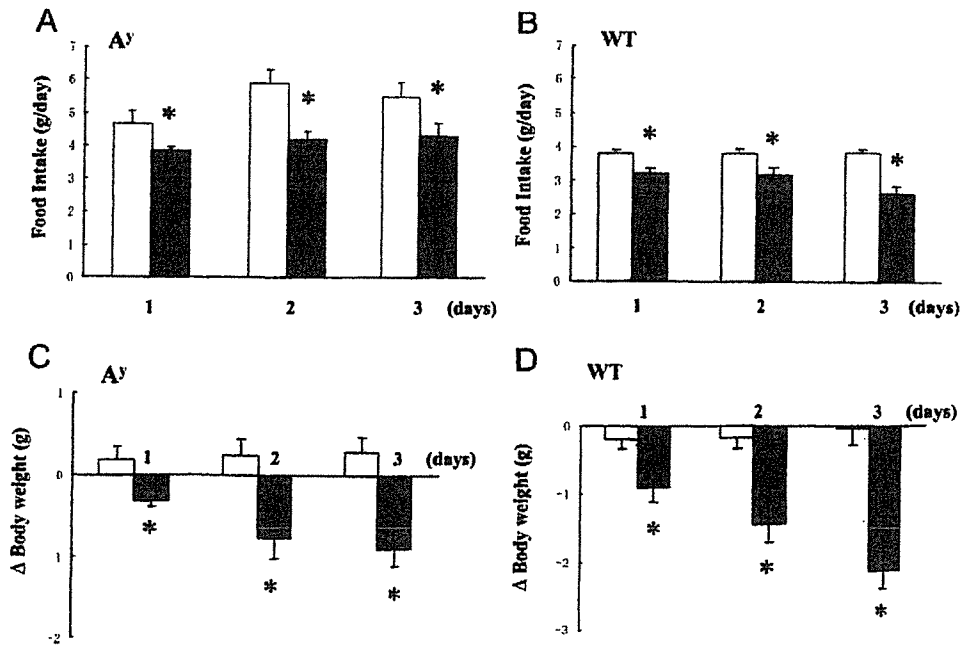

FIG. 7. Effects of chronic treatment with mCPP on food intake and body weight in 8-wk-old A^y mice (A and C) and wild-type (WT) mice (B and D). Each *column* and *bar* represents the mean value ± SEM of seven to nine mice. Basal body weight for wild-type, saline controls (*white bars*) was 29.0 ± 0.7 g; for the mCPP treatment group (*black bars*), 29.8 ± 0.3 g; for A^y mice, saline controls (*white bars*), 37.7 ± 0.5 g; and for the mCPP treatment group (*black bars*), 37.6 ± 0.5 g. *, $P < 0.05$.

ratio of active and des-acyl ghrelin. A^y mice have an agouti peptide-induced disturbance of the α-MSH ligand for MC-4 receptors that leads to hyperphagia (9, 10). These neuropeptides, therefore, are unlikely to contribute to hyperphagia, decreases in plasma des-acyl ghrelin levels, or the ratio of plasma active/des-acyl ghrelin in A^y mice.

We previously reported that fasting increases hypothalamic 5-HT2C and 5-HT1B receptor gene expression (30). In the present study, 5-HT2C and 5-HT1B receptor gene expression was increased in nonobese hyperphagic A^y mice and decreased by food restriction. The agouti peptide might therefore have an inhibitory role in hypothalamic 5-HT2C and 5-HT1B receptor gene expression under restricted feeding conditions. The increase in hypothalamic 5-HT2C and 5-HT1B receptor gene expression might be a compensatory response to hyperphagia induced by the agouti peptide in A^y mice, because 5-HT2C and 5-HT1B receptors have an inhibitory role in feeding (2–7). The present results also demonstrate that low plasma des-acyl ghrelin levels are not associated with alterations of hypothalamic NPY, AGRP, orexin, POMC, and CART gene expression in nonobese A^y mice. The increases in hypothalamic 5-HT2C and 5-HT1B receptor gene expression preceded the development of obesity in A^y mice, indicating that the induction of hypothalamic 5-HT2C and 5-HT1B receptor gene expression is not a secondary response to obesity and is independent of hypothalamic NPY, AGRP, orexin, POMC, and CART gene expression in A^y mice. Hypothalamic 5-HT2C and 5-HT1B receptor gene expression is likely to be inversely proportional to alterations of plasma des-acyl ghrelin in A^y mice and is altered by the feeding conditions.

Other investigators previously reported that A^y mice are resistant to the anorexic effects of fenfluramine (8). The present study, however, demonstrates that hyperphagic A^y mice are responsive to mCPP- and fenfluramine-induced appetite suppression. mCPP and fenfluramine increase hypothalamic POMC gene expression and POMC neuronal activity *in vivo* and *in vitro* (8, 30). 5-HT drugs such as mCPP and fenfluramine interact with POMC neurons in the hypothalamus and might stimulate POMC neurons to release enough α-MSH to overcome agouti blockade of MC receptors, because A^y mice are sensitive to MC agonist-induced feeding suppression (10). In addition, mCPP and fenfluramine increase hypothalamic CART gene expression (30). CART neurons have a different downstream pathway from MC (31, 32). POMC as well as CART might contribute to the anorexic effects of mCPP and fenfluramine.

The discrepancy between our results and previous results by other investigators might be because of the different methods used. Heisler *et al.* (33) examined the effects of fenfluramine on food intake for 50 min after ip fenfluramine injection. On the other hand, we administered the drugs ip, and 30 min later food was provided, and then we measured food intake for the next 1 h, because it usually takes about 30 min for drugs to act systemically after ip injection. The feeding state of mice might also contribute to the discrepancy. The present study demonstrates that the anorexic effects induced by stimulation of 5-HT2C and 5-HT1B receptors were attenuated in food-restricted A^y mice, but not in hyperphagic A^y mice. In a pharmacological study, Heisler *et al.* (33) used 4-wk-old A^y and wild-type mice, which might not have differed in food intake before the experiment. Restricted feeding for 3 d markedly reduced body weight, whereas treatment with mCPP slightly reduced body weight in A^y mice despite the suppression of feeding. mCPP-induced decreases in locomotor activity (33, 34) might contribute to this difference, because decreases in locomotor activity decrease energy expenditure.

In summary, these results suggest that the agouti peptide down-regulates hypothalamic 5-HT2C and 5-HT1B receptor gene expression under restricted feeding conditions and that chronic hyperphagia contributes to decreases in plasma des-acyl ghrelin levels and increases in hypothalamic 5-HT2C and 5-HT1B receptor gene expression in A^y mice. Hyperphagia predisposes A^y mice to obesity, hyperinsulinemia, and hyperglycemia.

Acknowledgments

Received April 3, 2006. Accepted September 6, 2006.

Address all correspondence and requests for reprints to: Katsunori Nonogaki M.D., Ph.D., Associate Professor, Center of Excellence, Division of Molecular Metabolism and Diabetes, Tohoku University Graduate School of Medicine, 2-1 Seiryou-machi, Aoba-ku, Sendai, Miyagi 980-8575, Japan. E-mail: knonogaki-tky@umin.ac.jp.

This work was supported by a Grant in-Aid for Scientific Research (C2) and Human Science Research (KH21016).

The authors have nothing to disclose.

References

1. **Simansky KJ** 1996 Serotonergic control of the organization of feeding and satiety. Behav Brain Res 73:37–42
2. **Tecott LH, Sun LM, Akana SF, Strack AM, Lowenstein DH, Dallman MF, Julius D** 1995 Eating disorder and epilepsy in mice lacking 5-HT2C serotonin receptors. Nature 374:542–546
3. **Nonogaki K, Strack AM, Dallman MF, Tecott LH** 1998 Leptin-independent hyperphagia and type 2 diabetes in mice with a mutated serotonin 5-HT2C receptor gene. Nat Med 4:1152–1156
4. **Nonogaki K** 2000 New insights into sympathetic regulation of glucose and fat metabolism. Diabetologia 43:533–549
5. **Vickers SP, Clifton PG, Dourish CT, Tecott LH** 1999 Reduced satiating effect of *d*-fenfluramine in serotonin 5-HT(2C) receptor mutant mice. Psychopharmacology 143:309–314
6. **Vickers SP, Dourish CT, Kennett GA** 2001 Evidence that hypophagia induced by *d*-fenfluramine and *d*-norfenfluramine in the rat is mediated by 5-HT2C receptors. Neuropharmacology 41:200–209
7. **Lee MD, Somerville EM, Kennett GA, Dourish CT, Clifton PG** 2004 Reduced hypophagic effects of *d*-fenfluramine and the 5-HT2C receptor agonist mCPP in 5-HT1B receptor knockout mice. Psychopharmacology 176:39–49
8. **Heisler LK, Cowley MA, Tecott LH, Fan W, Low MJ, Smart JL, Rubinstein M, Tatro JB, Marcus JN, Holstege H, Lee CE, Cone RD, Elmquist JK** 2002 Activation of central melanocortin pathways by fenfluramine. Science 297: 609–611
9. **Lu D. Willard D, Patel IR, Kadwell S, Overton L, Kost T, Luther M, Chen W, Woychik RP, Wilkison WO, Cone RD** 1994 Agouti protein is an antagonist of the melanocyte-stimulating-hormone receptor. Nature 371:799–802
10. **Fan W, Boston BA, Kesterson RA, Hruby VJ, Cone RD** 1997 Role of melanocortinergic neurons in feeding and the agouti obesity syndrome. Nature 385:165–168
11. **Ebihara K, Ogawa Y, Katsuura G, Numata Y, Masuzaki H, Satoh N, Tamaki M, Yoshioka T, Hayase M, Matsuoka N, Aizawa-Abe M, Yoshimasa Y, Nakao K** 1999 Involvement of agouti-related protein, an endogenous antagonist of hypothalamic melanocortin receptor, in leptin action. Diabetes 48: 2028–2033
12. **Boston BA, Blaydon KM, Varnerin J, Cone RD** 1997 Independent and additive effects of central POMC and leptin pathways on murine obesity. Science 278:1641–1644
13. **Wilson BD, Bagnol D, Kaelin CB, Ollmann MM, Gantz I, Watson SJ, Barsh GS** 1999 Physiological and anatomical circuitry between Agouti-related protein and leptin signaling. Endocrinology 140:2387–2397
14. **Martin NM, Houston PA, Patterson M, Sajedi A, Carmignac DF, Ghatei MA, Bloom SR, Small CJ** 2006 Abnormalities of the somatotrophic axis in the obese agouti mouse. Int J Obes 30:430–438